Xenophilic Complexes Bearing a Tp^R Ligand, $[Tp^R M{-}M'L_n]$ $[Tp^R{=}Tp^{iPr_2},$ $Tp^{\#}$ $(Tp^{Me_2,4\text{-}Br})$; M${=}$Ni, Co, Fe, Mn; $M'L_n{=}Co(CO)_4, Co(CO)_3(PPh_3),$ $RuCp(CO)_2]$: The Two Metal Centers are Held Together not by Covalent Interaction but by Electrostatic Attraction

Kazuhiro Uehara,[a] Shiro Hikichi,[a, b] Akiko Inagaki,[a] and Munetaka Akita*[a]

Dedicated to Professors Yoshihiko Moro-oka, Nobumasa Kitajima, and S. Jerry Trofimenko

Abstract: A series of dinuclear complexes, $[Tp^R M{-}M'L_n]$ $[Tp^{iPr_2}M{-}Co(CO)_4$ (**1**; M${=}$Ni, Co, Fe, Mn); $Tp^{\#}M{-}Co(CO)_4$ (**1′**; M${=}$Ni, Co); $Tp^{\#}Ni{-}RuCp(CO)_2$ (**3′**)] $(Tp^{iPr_2}{=}$hydrotris(3,5-diisopropylpyrazolyl)borato; $Tp^{\#}$ $(Tp^{Me_2,4\text{-}Br}){=}$hydrotris(3,5-dimethyl-4-bromopyrazolyl)borato), has been prepared by treatment of the cationic complexes $[Tp^{iPr_2}M(NCMe)_3]PF_6$ or the halo complexes $[Tp^{\#}M{-}X]$ with the appropriate metalates. Spectroscopic and crystallographic characterization of **1–3′** reveals that the tetrahedral, high-spin $Tp^R M$ fragment and the coordinatively saturated carbonyl–metal fragment $(M'L_n)$ are connected only by a metal–metal interaction and, thus, the dinuclear complexes belong to a unique class of xenophilic complexes. The metal–metal interaction in the xenophilic complexes is polarized, as revealed by their ν_{CO} vibrations and structural features, which fall between those of reference complexes: covalently bonded species $[R{-}M'L_n]$ and ionic species $[M'L_n]^-$. Unrestricted DFT calculations for the model complexes $[Tp^{H_2}Ni{-}Co(CO)_4]$, $[Tp^{H_2}Ni{-}Co(CO)_3(PH_3)]$, and $[Tp^{H_2}Ni{-}RuCp(CO)_2]$ prove that the two metal centers are held together not by covalent interactions, but by electrostatic attractions. In other words, the obtained xenophilic complexes can be regarded as carbonylmetalates, in which the cationic counterpart interacts with the metal center rather than the oxygen atom of the carbonyl ligand. The xenophilic complexes show divergent reactivity dependent on the properties of donor molecules. Hard (N and O donors) and soft donors (P and C donors) attack the $Tp^R M$ part and the ML_n moiety, respectively. The selectivity has been interpreted in terms of the hard–soft theory, and the reactions of the high-spin species **1–3′** with singlet donor molecules should involve a spin-crossover process.

Keywords: bond theory · density functional calculations · dinuclear complexes · metal–metal interactions · transition metals · xenophilic complexes

[a] Dr. K. Uehara, Prof. Dr. S. Hikichi, Dr. A. Inagaki,
Prof. Dr. M. Akita
Chemical Resources Laboratory
Tokyo Institute of Technology, R1–27
4259 Nagatsuta, Midori-ku, Yokohama 226–8503 (Japan)
Fax: (+81) 45-924-5230
E-mail: makita@res.titech.ac.jp

[b] Prof. Dr. S. Hikichi
Present address: Department of Applied Chemistry
School of Engineering, The University of Tokyo
Hongo, Bunkyo-ku, Tokyo 113–8656 (Japan)

Supporting information for this article is available on the WWW under http://www.chemeurj.org/or from the author. The information includes UV spectra for the series of $Tp^R Ni$ complexes, results of DFT calculations, preparative procedures for $Tp^{\#}Ni{-}Br$ and $Tp^{\#}Co{-}Cl$, and crystallographic data (details of measurements and structural analysis, tables of crystallographic data and selected structural parameters, and ORTEP views).
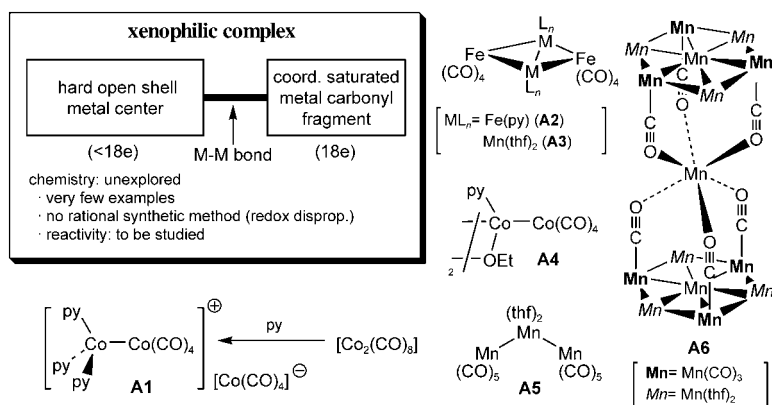
Introduction

Polar metal–metal bonds have attracted increasing attention,[1] because they are expected to display unique structural and reaction features based on a cooperative action of the two metal centers with different characters. Early–late heterobimetallic (ELHB) complexes have been studied extensively as typical examples of such compounds.[2] In addition to this category, a unique class of polynuclear complexes called "xenophilic complexes" is known.[3] A xenophilic complex is defined as a polynuclear complex, in which a hard open-shell metal center (frequently paramagnetic)[4] and a coordinatively saturated soft metal–carbonyl fragment are connected only through a metal–metal bond (Scheme 1), and the metal fragments with different electronic properties should form a polar metal–metal bond. In addition, xenophilic complex belongs to a family of coordinatively unsatu-

Scheme 1.

xenophilic complex

| hard open shell metal center | | coord. saturated metal carbonyl fragment |

(<18e)   M–M bond   (18e)

chemistry: unexplored
· very few examples
· no rational synthetic method (redox disprop.)
· reactivity: to be studied

L_n—M
Fe(CO)$_4$—M—Fe(CO)$_4$
L_n

[ML_n= Fe(py) (**A2**)
Mn(thf)$_2$ (**A3**)]

py
–/–Co—Co(CO)$_4$
–/–OEt   **A4**
$_2$

[py
py–Co—Co(CO)$_4$]$^\oplus$ py
py   ←——   [Co$_2$(CO)$_8$]
A1   [Co(CO)$_4$]$^\ominus$

(thf)$_2$
Mn   Mn
(CO)$_5$ (CO)$_5$
A5

Mn
Mn—|—Mn—Mn
Mn—C—Mn
Mn
C   C
‖   ‖
O   O
Mn
O   O
C   C
‖   ‖
Mn—|—C—Mn
Mn   Mn
Mn
A6
[**Mn**= Mn(CO)$_3$
Mn= Mn(thf)$_2$]

bled us to perform a systematic study on them. Herein we wish to report results of the study on synthesis, structure, and chemical properties of the [Tp^{R}M–M′L$_n$]-type xenophilic complexes containing the Co(CO)$_3$L and RuCp(CO)$_2$ fragments: [Tp^{R}M–Co(CO)$_4$] (**1/1′**), [Tp^{R}M–Co(CO)$_3$(PPh$_3$)] (**2**) [Tp^R=Tp^{iPr_2}, Tp$^\#$; M=Ni, Co, Fe, Mn], and [Tp$^\#$Ni–RuCp(CO)$_2$] (**3′**).[10,11] It is revealed that the two metal centers in the xenophilic complexes are held together not by covalent interaction, but by electrostatic attraction.

Results

Synthesis of xenophilic complexes 1–3′

Synthesis of [Tp^{iPr_2}M–Co(CO)$_4$] (1; M=Ni, Co, Fe, Mn) by treatment of [Tp^{iPr_2}M(NCMe)$_3$]PF$_6$ with PPN[Co(CO)$_4$]: We first attempted preparation of [Tp^{R}M–Co(CO)$_4$]-type complexes by metalation of the chloro precursors bearing the Tp^{iPr_2} and Tp^{Ph,Me} ligand[10] ([Tp^{R}M–Cl] M=Co, Ni) with the cobaltate (X$^+$[Co(CO)$_4$]$^-$ X=Na, K, PPN; PPN=bis(triphenylphosphine)iminium) in THF. However, the desired products could not be obtained.[12] Then in order to activate the Tp^{iPr_2}M fragments toward nucleophiles, the chloro complexes were converted to the labile, cationic, solvated complexes, [Tp^{iPr_2}M(NCMe)$_3$]$^+$PF$_6^-$ (**4**·PF$_6$)[14] by means of Cl$^-$ abstraction with a silver salt in acetonitrile. Treatment of the resultant **4**·PF$_6$ with PPN[Co(CO)$_4$] in CH$_2$Cl$_2$ afforded the desired dinuclear complexes, [Tp^{iPr_2}M–Co(CO)$_4$] (**1**; M=Ni, Co, Fe, Mn) (Table 1; entries 1–4).[15] Complexes **1** are sensitive to the air and moisture, but no apparent deterioration was observed if they were kept under an inert atmosphere.

Synthesis of [Tp$^\#$M–Co(CO)$_3$(L)] (Tp$^\#$=hydrotris(4-bromo-3,5-dimethylpyrazolyl)borato; M=Ni, Co; L=CO (1′), PPh$_3$ (2′)) by treatment of [Tp$^\#$M–X] with K[Co(CO)$_3$(L)]: In contrast to the reactions of the bulky Tp^R derivatives, synthesis of derivatives with the less bulky Tp$^\#$ ligand (Tp$^\#$: 3,5-dimethyl-4-bromo derivative; Table 1)[10] did not require prior conversion to the cationic precursors. Reaction of the halo complexes with K[Co(CO)$_4$] in THF gave the dinuclear complexes **1**$^{′Ni,Co}$ in moderate yields (Table 1; entries 5 and 6). Furthermore the bulkier cobaltate, [Co(CO)$_3$(PPh$_3$)]$^-$, could be introduced into the Tp$^\#$Ni system to afford **2**$^{′Ni}$ (entry 7).

Synthesis of [Tp$^\#$Ni–RuCp(CO)$_2$] (3′)—the first example of a xenophilic complex containing a second-row metal: The suc-

---

rated species,[5] which plays a key role in transformations mediated by organometallic species. The first examples of xenophilic complexes, including [(py)$_3$Co–Co(CO)$_4$]$^+$ [Co(CO)$_4$]$^-$ (**A1**[Co(CO)$_4$]), were formed by means of redox disproportionation of metal–carbonyl complexes by the action of pyridine as reported by Fachinetti (Scheme 1).[3b,c] Several examples of such compounds (**A**),[3] including a pentadecanuclear complex **A6**,[3f] have been reported so far, but all previously reported xenophilic complexes were formed through unpredictable redox disproportionation reactions of the metal centers. Furthermore their structure and reactivities, in particular the properties of the unique metal–metal bonds, have remained to be explored in a systematic manner.

In our laboratory inorganic and organometallic chemistry based on hydrotrispyrazolylborato (Tp^R) ligands has been a recent research subject.[6] The Tp^R ligand,[7] which is a facially coordinating tridentate N$_3$ ligand, is regarded as a tetrahedral enforcer, because the Tp^R ligand frequently forms a tetrahedral species, [(κ^3-Tp^R)M–X]. In the case of first-row transition metal complexes, a small ligand-field splitting brought about by the tetrahedral geometry often leads to a high-spin electronic configuration. Taking into account the unique properties of the Tp^R ligand, we carried out the systematic synthetic study of dioxygen complexes, which was followed by extension to organometallic systems. As a result, we succeeded in the preparation of highly coordinatively unsaturated hydrocarbyl complexes, [Tp^{R}M–R′], with 14 (Fe) and 15 (Co) valence electrons; these complexes did not undergo β-hydride elimination.[8] The successful synthesis of the hydrocarbyl complexes prompted us to introduce a metal fragment to obtain dinuclear complexes, [Tp^{R}M–M′L$_n$], which should be "xenophilic". A number of polynuclear complexes bearing a Tp^R ligand have been prepared, but none of them is xenophilic as their metal–metal bonds are supported by bridging ligands (e.g., μ-CO) or the Tp^{R}M moiety is coordinatively saturated due to coordination of additional auxiliaries (e.g., η^1-CO).[9] When we initiated the present study, no xenophilic complex with a Tp^R ligand was known.[9g] The first rational synthetic method reported herein provided a series of xenophilic complexes and ena-

Table 1. Reactions of $4 \cdot PF_6$ or $[Tp^R M-X]$ with $[M'L_n]$.

Entry	Tp^R	Precursor	M	$[M'L_n]^-$	Product	Yield [%]
1	Tp^{iPr_2}	$4 \cdot PF_6$	Ni	$PPN[Co(CO)_4]$	$[Tp^{iPr_2}Ni-Co(CO)_4]$ (1^{Ni})	55
2	Tp^{iPr_2}	$4 \cdot PF_6$	Co	$PPN[Co(CO)_4]$	$[Tp^{iPr_2}Co-Co(CO)_4]$ (1^{Co})	42
3	Tp^{iPr_2}	$4 \cdot PF_6$	Fe	$PPN[Co(CO)_4]$	$[Tp^{iPr_2}Fe-Co(CO)_4]$ (1^{Fe})	35
4	Tp^{iPr_2}	$4 \cdot PF_6$	Mn	$PPN[Co(CO)_4]$	$[Tp^{iPr_2}Mn-Co(CO)_4]$ (1^{Mn})	27
5	$Tp^\#$	$Tp^\#Ni-Br$	Ni	$K[Co(CO)_4]$	$[Tp^\#Ni-Co(CO)_4]$ ($1'^{Ni}$)	58
6	$Tp^\#$	$Tp^\#Co-Cl$	Co	$K[Co(CO)_4]$	$[Tp^\#Co-Co(CO)_4]$ ($1'^{Co}$)	53
7	$Tp^\#$	$Tp^\#Ni-Br$	Ni	$K[Co(CO)_3PPh_3]$	$[Tp^\#Ni-Co(CO)_3PPh_3]$ ($2'^{Ni}$)	36
8	$Tp^\#$	$Tp^\#Ni-Br$	Ni	$K[RuCp(CO)_2]$	$[Tp^\#Ni-RuCp(CO)_2]$ ($3'$)	41
9	$Tp^\#$	$Tp^\#Ni-Br$	Ni	$K[Mn(CO)_5]$	(see structure) ($5'$)	41

cessful direct synthesis of the $Tp^\#$ derivatives encouraged us to examine reactions with other metalates.

Reaction of $[Tp^\#Ni-Br]$ with $K[RuCp(CO)_2]$ in THF did not afford any characterizable product, but sonication of $[Tp^\#Ni-Br]$ and $K[RuCp(CO)_2]$ suspended in toluene gave the dinuclear complex $[Tp^\#Ni-RuCp(CO)_2]$ ($3'$; Table 1; entry 8). The obtained dark red complex $3'$ is the first example of a xenophilic complex containing a second-row metal fragment. Reaction of $[Tp^\#Co-Cl]$ gave a product that showed spectroscopic features different from those of $3'$, but could not be isolated in a pure form despite many attempts. Analogous reactions of $[Tp^\#Ni-Br]$ with $Na/K[FeCp(CO)_2]$ gave a product that showed two CO vibrations characteristic of the $FeCp(CO)_2$ fragment, but was too unstable to be isolated and characterized.

Reaction of $[Tp^\#Ni-Br]$ with $K[Mn(CO)_5]$ in THF overnight gave an anionic product, which was characterized after salt exchange ($5'$: NEt_4 salt) (Table 1; entry 9). The product $5'$, however, was not the desired product $[Tp^\#Ni-Mn(CO)_5]$, but the trinuclear complex with a linear Ni-Mn-Ni linkage as revealed by X-ray crystallography (SI 27[13]). The anionic part sits on a crystallographic centrosymmetric site (Ni-Mn-Ni: 180°; Ni1-Mn1: 2.419(1) Å) and each Mn-Ni bond is bridged by three CO ligands.

Through the synthetic methods mentioned above, eight examples of xenophilic complexes containing the $Tp^R M$ fragments ($1^{Ni,Co,Fe,Mn}$, $1'^{Ni,Co}$, $2'^{Ni}$, and $3'$) were prepared successfully.

Characterization of xenophilic complexes: The obtained xenophilic complexes were characterized by spectroscopic and crystallographic methods. Because the phosphine-substituted products $[Tp^R M-Co(CO)_3(PPh_3)]$ ($2/2'$) obtained from

$1/1'$ and PPh_3 (see below), also belong to the class of xenophilic complexes, their characterization is described together.

X-ray crystallographic characterization: All twelve xenophilic complexes that appear in this paper ($1^{Ni,Co,Fe,Mn}$, $1'^{Ni,Co}$, $2^{Ni,Co,Fe,Mn}$, $2'^{Ni}$, and $3'$) were characterized by X-ray crystallography. Their selected structural parameters are summarized in Table 2 (see also SI 12[13]) and, as typical examples, molecular structures of 1^{Ni}, $1'^{Ni}$, 2^{Ni}, $2'^{Ni}$, and $3'$ are shown in Figure 1.

$[Tp^{iPr_2}M-Co(CO)_4]$ (**1**) and $[Tp^\#M-Co(CO)_4]$ (**1'**): The six complexes **1** and **1'** with the virtually C_{3v}-symmetrical core structures with respect to the M–Co axis are isostructural, as shown by the molecular structures of 1^{Ni} and $1'^{Ni}$ (Figure 1; for the other complexes, see SI 16–18, and 20[13]), and their structural parameters are compared in Table 2.

The M–Co distances of about 2.5 Å are slightly longer than the sum of the covalent radii of M and Co (2.32 Å for Co–Co). In the case of the Co complexes $1^{Co}/1'^{Co}$, the Co–Co distances are comparable to those in $[Co_2(CO)_8]$ (2.522 Å),[16a,17] and $[Co_2(\mu\text{-}CH_2)(\eta^5\text{-}C_5H_4Me)_2(CO)_2]$ (2.497(1) Å)[16b] with bridging ligands (μ-CO, μ-CH_2), but substantially shorter than that in $[\{Co(CO)_3\{PPh_2(C_6H_4\text{-}CH_2NMe_2\text{-}o)\}\}_2]$ (2.702 Å),[16c] in which the two cobalt centers are connected by the covalent metal–metal bond only. The increase of the M–Co and M–N distances for the **1/1'** series is associated with the increase of the atomic radius of M, and replacement of Tp^{iPr_2} by the $Tp^\#$ ligand causes a slight shortening of the M–Co bond [**1/1'**: $\Delta = 0.05$ Å (M = Ni), 0.07 Å (M = Co)].[18] No apparent systematic change is observed for other structural parameters. The partial structures of the $Tp^R M$ and $Co(CO)_4$ moieties are similar to the structures of related mononuclear tetrahedral $Tp^R M-X$ species and trigonal-bipyramidal $X-Co(CO)_4$ species, respectively. The Tp^R ligands are κ^3-coordinated to the metal center; the differences in the three M–N distances for each complex are less than 0.045 Å and the ∢Co-M-N angles are in the range of 119–130° indicating C_{3v}-symmetrical structures. The equatorial CO ligands of the trigonal bipyramidal Co centers are tilted toward the nickel center as judged by the M-Co-CO angles (74.3–85.4°), but the linear Co-C-O linkage (>174.1°) and the M···CO distances longer than 2.6 Å reveal that the CO ligands are virtually η^1-bonded to Co without any substantial bonding interaction with M, leaving the $Tp^R M$ moiety electron-deficient as in the hydro-

Table 2. Selected structural parameters for xenophilic complexes [$Tp^R M-M'L_n$] **1–3**′.[a]

	1[Ni][b]	**1**[Co][b]	**1**[Fe]	**1**[Mn]	**1**′[Ni]	**1**′[Co]
M–M′	2.4640(8)	2.4969(8)	2.504(1)	2.582(1)	2.4190(9)	2.4467(9)
M–N [c]	2.002(4)	2.030(3)	2.057(5)	2.120(4)	2.011(4)	2.049(4)
M′-CO [c]	1.760(6)	1.764(5)	1.777(7)	1.767(7)	1.766(7)	1.784(7)
M′-C4(P1)	1.786(6)	1.793(5)	1.795(7)	1.783(7)	1.790(6)	1.773(5)
M⋯C1	2.826(4)	2.843(3)	2.954(6)	2.978(7)	2.859(6)	2.764(6)
M⋯C2	2.661(4)	2.684(3)	2.671(7)	2.707(7)	2.608(6)	2.745(6)
M⋯C3	2.661(4)	2.684(3)	2.667(6)	2.716(6)	2.594(6)	2.678(5)
M-M′-C1	82.2(2)	81.8(2)	85.4(2)	84.3(2)	84.5(2)	80.2(2)
M-M′-C2	76.1(1)	75.9(1)	75.0(2)	74.3(2)	75.3(2)	79.2(2)
M-M′-C3	76.1(1)	75.9(1)	75.1(2)	74.7(2)	74.9(2)	77.0(2)
M-M′-C4(P1)	176.1(2)	176.8(2)	172.4(2)	172.4(2)	173.1(2)	177.7(2)
B⋯M-Co	179.2(1)	179.55(9)	177.2(1)	177.2(1)	175.1(8)	179.03(9)
N11-M-M′-CO [c]	60.4(1)	59.6(1)	63.0(3)	62.8(3)	64.1(2)	59.3(2)
C1-M′-P-C(Ph) [c]	–	–	–	–	–	–

	2[Ni]	**2**[Co]	**2**[Fe]	**2**[Mn]	**2**′[Ni]	**3**′
M–M′	2.4138(9)	2.4236(7)	2.4465(6)	2.5113(6)	2.3768(9)	2.512(1)
M–N[c]	2.006(6)	2.063(4)	2.081(3)	2.126(3)	2.019(5)	2.039(6)
M′-CO[c]	1.75(1)	1.763(5)	1.761(5)	1.756(4)	1.769(7)	1.855(8)
M′-C4(P1)	2.198(2)	2.194(1)	2.1854(9)	2.1864(8)	2.195(2)	–
M⋯C1	2.860(8)	2.927(5)	2.926(4)	2.962(4)	2.964(6)	2.866(9)
M⋯C2	2.751(8)	2.788(5)	2.811(4)	2.829(3)	2.663(6)	2.761(8)
M⋯C3	2.622(9)	2.537(4)	2.552(4)	2.613(3)	2.479(6)	–
M-M′-C1	85.0(2)	87.0(1)	86.4(1)	85.8(1)	90.0(2)	80.4(3)
M-M′-C2	80.9(2)	81.9(1)	82.2(1)	81.0(1)	78.4(2)	76.8(3)
M-M′-C3	76.3(2)	72.8(1)	72.7(1)	73.2(1)	71.8(2)	–
M-M′-C4(P1)	172.23(7)	166.48(5)	166.44(4)	167.11(4)	160.06(6)	–
B⋯M-Co	177.5(1)	175.8(1)	175.60(9)	174.70(8)	174.2(1)	172.4(1)[d]
N11-M-M′-CO[c]	61.1(4)	61.9(2)	61.7(2)	61.9(1)	64.0(3)	47.0(3)
C1-M′-P-C(Ph)[c]	61.5(4)	60.2(3)	60.3(2)	60.2(2)	63.7(3)	–

[a] Interatomic distances in Å and bond angles and dihedral angles in degrees. [b] Mirror-symmetrical structures. [c] Averaged values. [d] ∡B⋯Ni–Ru.

carbyl complexes.[8] Thus the two metal fragments in **1**/**1**′ are connected solely by the metal–metal interaction. The M−Co vector is superimposed on the threefold axis of the $Tp^R Ni$ moiety as judged by the B1⋯M−Co1 angle (175.18–179.55°), and the staggered conformation of the three pz^R rings and the three equatorial CO ligands is evident from the N11-M-Co-CO dihedral angles close to 60° and can also been clearly seen in the bottom view of **1**[Ni] (Figure 1).

[Tp^{iPr_2}M−Co(CO)_3(PPh_3)] (2) and [Tp^#M−Co(CO)_3(PPh_3)] (2′): Structural features similar to those noted for the CO derivatives **1**/**1**′ are observed for the PPh₃-substituted products **2**/**2**′. ORTEP views for **2**[Ni] and **2**′[Ni] are shown in Figure 1 (For the other PPh₃-complexes, see the SI 22–24[13]).

Replacement of the axial CO ligand by PPh₃ causes a slight shortening of the M−Co lengths: **1**/**2** [$\Delta = 0.05$ Å (M = Ni), 0.07 Å (M = Co), 0.04 Å (M = Fe), 0.07 Å (M = Mn)]. It is notable that the core structures are slightly distorted from a C_{3v}-symmetrical structures to an apparent C_s-symmetrical structure as indicated by 1) bending of the M-Co-P linkage [160.06–172.23° (av 166.5°); cf. **1**: 172.4–176.8° (av 174.4°), **1**′: 173.1–177.7° (av 175.4°)], 2) the M-Co-C3 angles being more acute than the M-Co-C1,2 angles, 3) deviation of the M1-C3-O3 moiety from a linear structure (173.4–175.5°; cf. **1**, **1**′: 175.7–177.3°), and 4) the unsymmetrical M⋯CO distan-

ces (M⋯C3 < M⋯C1, M⋯C2). This distortion will be analyzed by DFT calculations (see below).

[Tp^#M−RuCp(CO)_2] (3′): The tetrahedral $Tp^#Ni$ fragment and the $RuCp(CO)_2$ fragment with a three-legged piano-stool structure are connected by the Ni−Ru bond. As is evident from a view along the Ru−Ni axis (Figure 1), the three ligands on Ru (2 CO, Cp) and the three pz^R rings on Ni are arranged in a staggered conformation to avoid steric repulsions among them, leading to a pseudo-C_3-symmetrical structure. The length of the unsupported Ni−Ru bond (2.512(1) Å) is slightly shorter than those in the coordinatively saturated adducts with additional bridging ligands (2.56–2.57 Å (**18**′, **19**′); see below). The CO ligands are η¹-bonded to the Ru center with no bridging interaction with the Ni center as is also evident from the linear Ru-C-O linkage (Ru-C1-O1: 175.9(8)°; Ru-C2-O2: 176.5(8)°) and the Ni⋯CO separations (Ni1⋯C1: 2.866(9) Å; Ni1⋯C2: 2.761(8) Å).

Spectroscopic characterization: Spectroscopic data for the xenophilic complexes **1–2**′ are summarized in Table 3 and the data for **3**′ is shown in the experimental part.

IR spectra: IR data is useful in discussing geometrical features and electronic structures of xenophilic complexes. For complexes **1**/**1**′ and **2**/**2**′, 1) the ν_{CO} patterns[19] (KBr, CH_2Cl_2) peculiar to C_{3v}-symmetrical, trigonal-bipyramidal structures (X-Co(CO)₄: three intense vibrations; X-Co(CO)₃(L): two intense vibrations) and 2) the ν_{BH} bands above 2500 cm⁻¹ indicative of κ^3-Tp^R coordination[20] are in accord with the desired C_{3v}-symmetrical structures consisting of the Co(CO)₃(L) and (κ^3-Tp^R)M fragments. An IR spectrum for **3**′, containing two CO vibrations characteristic of the RuCp(CO)₂ fragment (1953, 1891 cm⁻¹ (KBr)) in addition to the ν_{BH} band at 2553 cm⁻¹ (κ^3-$Tp^#$),[20] is also consistent with the structure characterized by X-ray crystallography (Figure 1). It is notable that 1) no CO vibration below 1900 cm⁻¹ (KBr, CH_2Cl_2) is detected, indicating lack of a bridging CO ligand; and 2) for a certain series of complexes, the ν_{CO} absorptions are very similar irrespective of M (e.g., **1**[M] series: ν_{CO} 2051 ± 1, 1980 ± 2, 1934 ± 3 cm⁻¹).
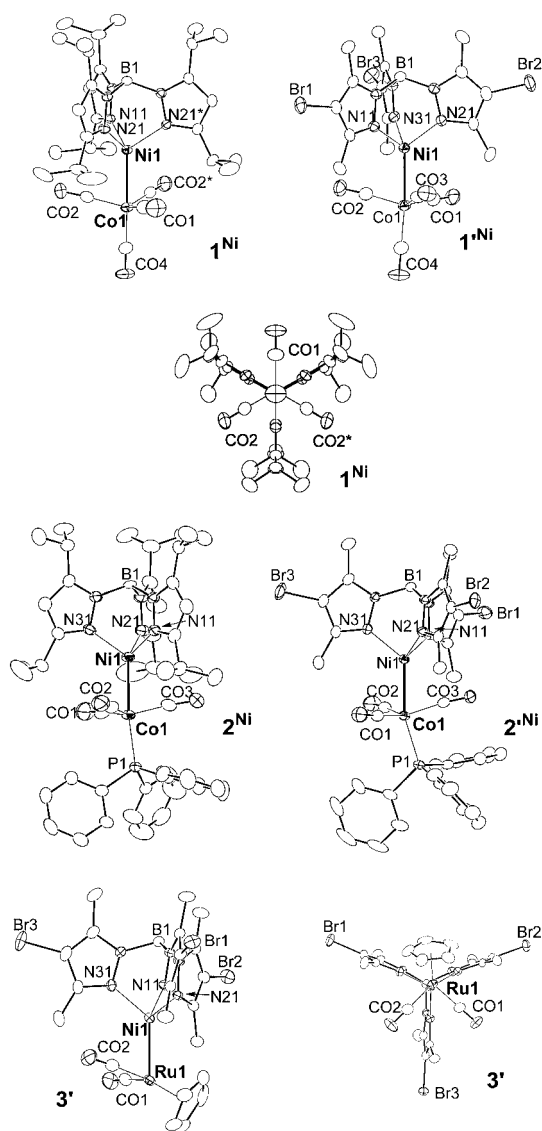
Figure 1. Molecular structures of the xenophilic complexes drawn with thermal ellipsoids at the 30% probability level.

A significant solvent effect was noted. The results are summarized in Table 3 and typical IR spectra for 1^{Ni} are shown in Figure 2. Solution IR spectra of $1/1'$ observed in CH_2Cl_2 were similar to those recorded as KBr pellets. In sharp contrast to these IR spectra, those observed in MeCN showed completely different features; no absorption was observed above 1900 cm^{-1} and instead a single intense band appeared at 1892 cm^{-1}. This drastic change in the IR spectrum was accompanied by color change from purple red (solid and in CH_2Cl_2) to blue (in MeCN); for results of the UV-visible measurements, see below. The lower energy ν_{CO} band observed in MeCN suggested formation of an anionic species, which was characterized as the $[Co(CO)_4]^-$ ion and was confirmed by comparison with an authentic sample of the isolable PPN$[Co(CO)_4]$.[21] It should be noted that re-

moval of MeCN under reduced pressure regenerated the IR absorptions of 1^{Ni} (KBr), although partial decomposition was evident. These observations revealed that dissolution of $1/1'$ in MeCN caused heterolysis of the M–Co bonds to give the ion pairs $4/4'[Co(CO)_4]$ (Scheme 2). The IR spectra of $1/1'$ observed in THF contained two sets of signals attributable to $1/1'$ and $[4/4'(thf)][Co(CO)_4]$, suggesting that the two species were present as an equilibrated mixture.

The PPh$_3$-substituted derivatives $2/2'$ exhibited IR features similar to those of $1/1'$. Dissolution in a 1:1 MeCN/CH_2Cl_2 mixture (CH_2Cl_2 was added to dissolve $2/2'$) caused heterolytic cleavage of the M–Co bonds as judged by the appearance of the absorptions assignable to $[Co(CO)_3(PPh_3)]^-$, but dissolution in CH_2Cl_2 or THF did not cause any spectral change. Retention of the M–Co bond in THF should result from the relative instability (pK_b) of $[Co(CO)_3(PPh_3)]^{-[22]}$ with respect to $[Co(CO)_4]^-$.

The Ru–Ni complex $3'$ showed two CO vibrations characteristic of the RuCp(CO)$_2$ fragment when observed as a KBr pellet or in CH_2Cl_2, but decomposed upon dissolution in MeCN as judged by IR. Complex $[RuCp(CO)_2]_2$ (D), which was detected as the only characterizable component, might be formed through oxidative dimerization of $[RuCp(CO)_2]^-$ resulting from a Ni–Ru bond heterolysis.

The significant solvent effects observed for $1/1'$ and $2/2'$ suggest a polar nature of the M–Co bonds in them.

UV-visible and ^{1}H NMR spectra, and magnetic susceptibility: UV-visible data for $1/1'$ and $2/2'$ are summarized in Table 3 and, as typical examples, UV-visible spectra for the series of the Tp^{R}Ni complexes are shown in the Supporting Information (SI 1[13]). The absorptions below about 500 nm, which are common for the Tp^{R}Ni–X-series complexes including Tp^{iPr_2}Ni–Cl, are assigned to d–d transitions of tetrahedral, high-spin Tp^{R}Ni–X species.[23]

Introduction of the PPh$_3$ ligand ($2/2'$) causes appearance of new absorptions around 400 nm, which could be ascribed either to ligand–metal charge-transfer (LMCT) bands of the Co–P moiety or to metal–metal charge-transfer (MMCT) bands.[24] The replacement of CO with PPh$_3$ in complexes of Fe and Mn ($1^{Fe,Mn}$), which are virtually transparent in the lower energy region (> 350 nm), causes appearance of new bands in the same region (Table 3). Therefore, the bands around 400 nm can be assigned to LMCT bands of the Co(CO)$_3$(PPh$_3$) fragment.
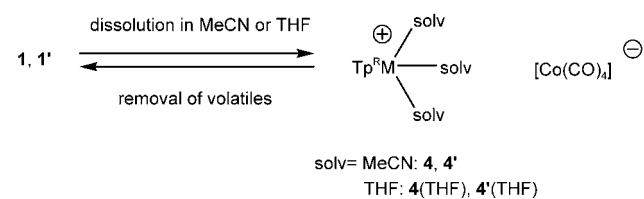
A dramatic change was observed upon replacing the solvent from CH_2Cl_2 to MeCN in accord with the change observed by IR (Figure 2). The weakening of the d–d transitions was consistent with the conversion into an octahedral species (Scheme 2) and the spectra observed in MeCN were essentially identical to those of $4\cdot$PF$_6$, the starting compounds. Complex PPN$[Co(CO)_4]$ did not show any intense absorption in this region.

All xenophilic complexes obtained are paramagnetic, and paramagnetically shifted ^{1}H NMR spectra consistent with the composition of the xenophilic complexes were obtained (see the Experimental Section).

Table 3. Selected spectroscopic data for xenophilic complexes **1–2'**.

	KBr		CH$_2$Cl$_2$	THF	CH$_3$CN [a]	UV/Vis: λ [nm] (ε [cm^{-1} mol^{-1}])[b]
	ν_{BH}	ν_{CO}	ν_{CO}	ν_{CO}	ν_{CO}	
1^{Ni}	2534	2052 (s), 1982 (vs), 1937 (vs)	2051, 1980, 1947	2051, 1980, 1941, 1885	1892	488 (230), 544 (460), 867 (90), 922 (100)
1^{Co}	2537	2052 (s), 1982 (s), 1935 (vs)	2052, 1979, 1946	2052, 1979, 1943, 1885	1892	459 (410), 640 (380), 666 (460), 690 (sh, 340), 913 (60)
1^{Fe}	2536	2051 (s), 1980 (s), 1932 (vs)	2051, 1978, 1944	2051, 1978, 1941, 1885	1892	[c]
1^{Mn}	2539	2052 (s), 1979 (vs), 1935 (vs)	2052, 1977, 1941	2051 1977, 1938, 1885	1892	[c]
1'^{Ni}	2546	2062 (vs), 1993 (vs), 1951 (vs), 1934 (vs)	2057, 1986, 1948	2057, 1987, 1945,[d] 1885	1893	337 (1143), 400 (741), 543 (835), 852 (135), 941 (162)
1'^{Co}	2544	2062 (s), 1993 (s), 1953 (vs), 1935 (vs)	2056, 1987, 1947	2069, 2038,[d] 1885	1893	366 (2625), 466 (759), 666 (500)
2^{Ni}	2534	1979 (m), 1907 (vs), 1896 (vs)	1978, 1905, 1892	1978, 1956, 1905, 1897	1927, 1892, 1838	404 (720), 520 (630), 955 (130)
2^{Co}	2544	1973 (m), 1899 (vs), 1884 (vs)	1978, 1954, 1905, 1889	1978, 1956, 1905, 1897	1927, 1840, 1837	386 (1200), 508 (390), 678 (540), 901 (30)
2^{Fe}	2545	1970 (m), 1894 (vs), 1879 (vs)	1975, 1956, 1903, 1885	1975, 1956, 1903, 1890	[e]	391 (3980), 653 (49)
2^{Mn}	2549	1970 (m), 1893 (vs), 1878 (vs)	1975, 1899, 1881	1974, 1956, 1887	[e]	393 (3940), 678 (260)
2'^{Ni}	2544	1979 (m), 1905 (vs), 1882 (vs)	1979, 1906	1979, 1957, 1906	1927, 1894, 1837	417 (983), 514 (1051), 983 (179)

[a] PPh$_3$ complexes **2** were recorded in CH$_2$Cl$_2$/CH$_3$CN (1:1), because they were sparingly soluble in MeCN. [b] Recorded in CH$_2$Cl$_2$. [c] No characteristic absorption. [d] Very weak signals. [e] Decomposed.
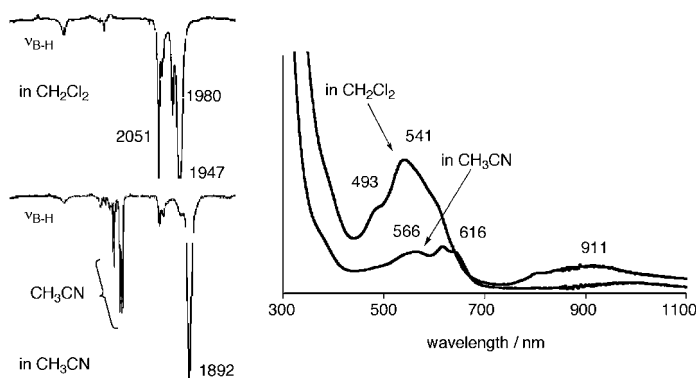
Figure 2. IR and UV spectra of **1^{Ni}** observed in CH$_2$Cl$_2$ and CH$_3$CN.

Scheme 2.

The effective magnetic moments (μ_{eff}) of **1^{Ni}** (2.75 μ_B), **1'^{Ni}** (3.06 μ_B), **2^{Ni}** (3.16 μ_B), **2'^{Ni}** (2.97 μ_B), **1'^{Co}** (3.89 μ_B), and **2^{Co}** (4.47 μ_B) indicate high-spin electronic configurations ($S = 3/2$ (Co), 1 (Ni)) as reported for the alkyl complexes,[8] but that of **1^{Co}** (2.37 μ_B) is smaller than the expected spin-only value, although other spectroscopic features of **1^{Co}** are very similar to those of **1'^{Co}**.[25] The reason is not clear at present. The Ni–Ru complex **3'** also turns out to be a triplet species ($\mu_{eff} = 2.92$).

The crystallographic and spectroscopic analyses reveal that in the dinuclear complexes **1/1'**, **2/2'**, and **3'**, the tetrahe-
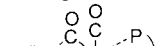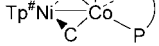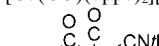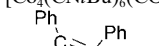
dral, hard open-shell, high-spin metal fragment (MTp^R) and the coordinatively saturated metal carbonyl fragment (M'L$_n$) with the trigonal-bipyramidal structures [Co(CO)$_3$(L)] or the three-legged piano-stool structure [RuCp(CO)$_2$] are connected by a metal–metal bond, leading to the characterization as "xenophilic complexes". The cobalt complexes **1^{Co}** and **1'^{Co}** are isoelectronic with **A1** (Scheme 1). It is worth noting that for a certain series of complexes, their core structures and their CO vibrations are very similar irrespective of M.

Divergent reactivity of xenophilic complexes toward nucleophiles: In order to characterize the reactivity of the xenophilic complexes, as typical examples, complexes **1^{Ni,Co}**, **1'^{Ni,Co}**, and **3'** were subjected to reactions with donor molecules.[25] As a result, the xenophilic complexes showed divergent reactivity, which was dependent on the properties of the donor molecules: hard versus soft.

Reactivity of [Tp^{R}M−Co(CO)$_4$] (1 and 1'): The results will be described with the emphasis on the Tp$^#$ system (**1'**), because the Tp^{iPr_2} complexes (**1**) were sluggish, presumably due to the bulky Tp^{iPr_2} ligand and frequently gave a mixture of products.

Reaction with hard donors—heterolytic cleavage of the M−M interaction giving ion pairs: Reaction of the NiTp$^#$ complex **1'^{Ni}** with hard N- and O-donors (D) in CH$_2$Cl$_2$ caused Ni–Co bond heterolysis to give the ion pairs (Table 4) in a manner similar to the phenomenon observed upon dissolution of **1/1'** in MeCN (Scheme 2). The products were fully characterized by spectroscopic and crystallographic methods. The anionic part was readily determined to be [Co(CO)$_4$]$^-$ on the basis of the strong ν_{CO} vibration around 1890 cm^{-1}. The drastic color change suggested a change of the coordination geometry of the Tp$^#$Ni moiety, which was confirmed by X-ray crys-

Table 4. Reaction of [Tp^RM−Co(CO)$_4$] with donors (D) in CH$_2$Cl$_2$.

Tp^R	M	D	Product	Yield
$Tp^\#$	Ni	4-*tert*-butylpyridine	[$Tp^\#$Ni(D)$_3$][Co(CO)$_4$] (**6'^{Ni}**)	78
$Tp^\#$	Co	4-*tert*-butylpyridine	[$Tp^\#$Co(D)$_3$][Co(CO)$_4$] (**6'^{Co}**)	39
$Tp^\#$	Ni	diphenylcyclopropenone	[$Tp^\#$Ni(D)$_3$][Co(CO)$_4$] (**7'^{Ni}**)	69
$Tp^\#$	Co	diphenylcyclopropenone	[$Tp^\#$Co(D)$_3$][Co(CO)$_4$] (**7'^{Co}**)	38
$Tp^\#$	Ni	4-methylpyridine oxide	[$Tp^\#$Ni(D)$_3$][Co(CO)$_4$] (**8'^{Ni}**)	83
$Tp^\#$	Co	4-methylpyridine oxide	[$Tp^\#$Co(D)$_3$][Co(CO)$_4$] (**8'^{Co}**)	56
$Tp^\#$	Ni	DMSO	[$Tp^\#$Ni(dmso)$_2$(OH$_2$)][Co(CO)$_4$] (**9'^{Ni}**)	66
$Tp^\#$	Co	DMSO	[$Tp^\#$Co(dmso)$_2$(OH$_2$)][Co(CO)$_4$] (**9'^{Co}**)	47
$Tp^\#$	Ni	2,2'-bipyridyl	[$Tp^\#$Ni(D)−Co(CO)$_4$] (**10'a^{Ni}**)	83[a]
$Tp^\#$	Ni	4,4'-dimethyl-2,2'-bipyridyl	[$Tp^\#$Ni(D)−Co(CO)$_4$] (**10'b^{Ni}**)	62[a]
Tp^{iPr_2}	Ni	PPh$_3$	[Tp^{iPr_2}Ni−Co(CO)$_4$(PPh$_3$)] (**2^{Ni}**)	35
Tp^{iPr_2}	CO	PPh$_3$	[Tp^{iPr_2}Co−Co(CO)$_4$(PPh$_3$)] (**2^{Co}**)	51
Tp^{iPr_2}	Fe	PPh$_3$	[Tp^{iPr_2}Fe−Co(CO)$_4$(PPh$_3$)] (**2^{Fe}**)	12
Tp^{iPr_2}	Mn	PPh$_3$	[Tp^{iPr_2}Mn−Co(CO)$_4$(PPh$_3$)] (**2^{Mn}**)	17
$Tp^\#$	Ni	PPh$_3$	[$Tp^\#$Ni−Co(CO)$_4$(PPh$_3$)] (**2^{Ni}**)	36
Tp^{iPr_2}	Ni/Co	dppe/deppene[b]	decomposition	
$Tp^\#$	Ni	dppe	(**11'a**)	48
$Tp^\#$	Ni	deppene[b]	(**11'b**)	45
$Tp^\#$	Co	dppe	[Co(CO)(dppe)$_2$][Co(CO)$_4$]$_2$ (**12**)	11
$Tp^\#$	Ni	*t*BuNC	(**13'**)	77
$Tp^\#$	Co	*t*BuNC	[Co$_4$(CN*t*Bu)$_6$(CO)$_6$] (**14**)	trace
$Tp^\#$	Ni	PhC≡CPh	(**15'**)	9

[a] M = Co; decomposition. [b] dppene = *cis*-1,2-bis(diphenylphosphino)ethene.

tallography (SI 28–32[13]). The cationic parts of the products obtained from 4-*tert*-butylpyridine (**6'^{Ni}**), diphenylcyclopropenone (**7'^{Ni}**),[26] and 4-methylpyridine oxide (**8'^{Ni}**) are octahedral tris(ligand)-coordinated species, whereas those obtained from DMSO (**9'^{Ni}**; *O*-coordinated), 2,2'-bipyridyl (**10'a^{Ni}**), and 4,4'-dimethyl-2,2'-bipyridyl (**10'b^{Ni}**) contain another donor molecule, that is, the aquo ligand in **9'^{Ni}** and the isocarbonyl ligand in **10'a,b^{Ni}**[27] to furnish the octahedral 2+1 adducts.

The products **6'^{Co}**–**9'^{Co}** obtained from the cobalt complex **1^{Co}** are isostructural with the corresponding nickel derivatives, as their IR spectra are virtually identical to those of **6'^{Ni}**–**9'^{Ni}**. The reaction of **1^{Co}** with bipy gave an intractable mixture of products.

Reaction with soft donors—ligand substitution and addition at the Co(CO)$_4$ moiety: Soft donors gave different types of products as summarized in Table 4.

Addition of PPh$_3$ to a solution of **1/1'** in toluene caused vigorous gas evolution (CO), and the products were isolated by crystallization from toluene/pentane. Characterization of the PPh$_3$-substituted derivatives **2/2'** is described above.

Reaction of the NiTp$^\#$ complex **1'^{Ni}** with diphosphines gave the chelated products **11'a,b**, and an analogous product **13'** was obtained from *t*Bu−NC. The diamagnetic products

11' and **13'** were characterized on the basis of their spectroscopic features: 1) κ^3-$Tp^\#$ (ν_{BH} > 2500 cm^{-1}),[20] 2) shift of CO ligands to the bridging sites (ν-(μ-CO)), and 3) elimination of one of the CO ligands. Reaction with Ph−C≡C−Ph gave the μ-η^2:η^2-adduct **15'**. X-ray crystallography of **11'a**, **13'**, and **15'** (SI 33, 34, and 36[13]) reveals that the $Tp^\#$ complexes are isostructural with the corresponding Cp derivatives, [CpNi−Co(CO)(D)$_2$(μ-CO)$_2$].[28] The reaction of the Tp^{iPr_2} complex **1^{Ni}** with diphosphines, however, gave a complicated mixture of products, from which no characterizable compound could be isolated.

In contrast to the reactions of the $Tp^\#$Ni complex **1'^{Ni}**, those of the cobalt derivative **1'^{Co}** afforded very complicated mixtures, except for the reaction with PPh$_3$. Products isolated in low yields did not contain the $Tp^\#$ ligand. The reactions with 1,2-bis(diphenylphosphino)ethane (dppe) and *t*Bu−NC gave the ion pair **12** and the tetranuclear cluster compound **14** (SI 35[13]), respectively, which were apparently formed through the redox disproportionation of the Co(CO)$_4$ fragment in **1'^{Co}** induced by the added donors.
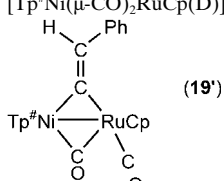
Reactivity of [$Tp^\#$Ni−RuCp(CO)$_2$] (3')

Stability of 3': Complex **3'** was much less stable toward the air and moisture than the Co(CO)$_4$ derivatives **1/1'**. Addition of water to **3'** gave a mixture of the dinuclear μ-pyrazolato complex, [(μ-pz$^\#$)(μ-OH)(NiTp$^\#$)$_2$] (**16'**) (SI 37[13]) and [RuCp(CO)$_2$]$_2$ (**D**), which should be formed through hydrolysis of the metal–metal bond followed by condensation of the resultant [(Tp$^\#$Ni)$_2$(μ-OH)$_2$] with pyrazole and oxidative dehydrogenation of [H−RuCp(CO)$_2$], respectively. Partial hydrolysis of the Tp^R ligand giving pyrazole was frequently observed during chemical reactions of Tp^RM complexes.[29] The difference in the stability of **1/1'** and **3'** toward moisture should result from the properties of the M'L$_n$ moiety; [RuCp(CO)$_2$]$^-$ is much more basic than [Co(CO)$_4$]$^-$.[30] Dissolution of **3'** in MeCN and acetone caused decomposition and no product other than **D** could be characterized.

Reactions with hard donors: Treatment of **3'** with hard donors (4-*tert*-butylpyridine, bipyridine, pyridine oxide, and diphenylcyclopropenone) in CH$_2$Cl$_2$ gave a mixture of the

octahedral chloronickel species coordinated by two donor molecules, [Tp#NiCl(D)$_2$] (**17′**), and [RuCp(CO)$_2$]$_2$ (**D**) (Table 5).[31] Simple crystallization of a reaction mixture obtained from **3′** and bipy gave co-crystals consisting of **17′b** and [RuCp(CO)$_2$]$_2$ (**D**) (SI 38[13]).[32] The molecular structure of the pyridine oxide adduct **17′c** was determined by X-ray crystallography (SI 39[13]), and the other products **17′a,d** were characterized on the basis of their IR spectra and elemental analysis.

The core parts of complexes **18′a,b** revealed by X-ray crystallography (SI 40 and 41[13]) are isostructural; coordination of the added donor to the Ru center causes the shift of two η^1-CO ligands to the bridging sites to form the coordinatively saturated diamagnetic species. The coordination mode of the Tp# ligand in **18′d** (SI 43[13]) is changed to κ^2 so as to release steric repulsion with the bulky PPh$_3$ ligand. In the case of **19′** the vinylidene ligand resulting from a 1,2-hydrogen shift of phenylacetylene bridges the two metal centers.[35]

Thus the reaction of **3′** with soft two-electron donors results in coordination to the Ru center rather than CO substitution as observed for the Co(CO)$_4$ derivatives **1/1′**.

Reaction with isothiocyanate: To examine the possibility of insertion of an unsaturated organic substrate into the Ni−Ru bond in **3′** a variety of heterocumulenes were treated with **3′**.[2,26] Reaction with isothiocyanates proceeded smoothly (Scheme 3), whereas CO$_2$, CS$_2$, and carbodiimide (Me$_3$Si−N=C=N−SiMe$_3$) gave intractable mixtures of products as observed for the reaction with MeCN and acetone. Fractional crystallization of the reaction mixtures gave the iminodithiocarbonato complexes **20′** in addition to the isonitrile complexes **18′** (Table 5). X-ray crystallography of **20′b,e** revealed the μ-κ^1(S;Ru):κ^2(N,S;Ni)-iminodithiocarbonato structure (SI 44 and 45[13]).

The compositions of the two products, that is, **20′** and **18′**, suggest that these products arise from disproportionation of two molecules of R−N=C=S into the iminodithiocarbonato ligand [(R−NCS$_2$)$^{2-}$] and isocyanide (R−NC); this reaction

Table 5. Reaction of [Tp#Ni−RuCp(CO)$_2$] with donors (D) in CH$_2$Cl$_2$.

D	Product	Yield
4-*tert*-butylpyridine	[Tp#Ni(D)$_2$Cl] (**17′a**) + [{RuCp(CO)$_2$}$_2$] (**D**)	34
bipyridine	[Tp#Ni(D)$_2$Cl] (**17′b**) + [{RuCp(CO)$_2$}$_2$] (**D**)	37
pyridine oxide	[Tp#Ni(D)$_2$Cl] (**17′c**) + [{RuCp(CO)$_2$}$_2$] (**D**)	13
diphenylcyclopropenone	[Tp#Ni(D)$_2$Cl] (**17′d**) + [{RuCp(CO)$_2$}$_2$] (**D**)	36
CO	[Tp#Ni(μ-CO)$_2$RuCp(D)] (**18′a**)	34
CyNC	[Tp#Ni(μ-CO)$_2$RuCp(D)] (**18′b**)	39
*t*BuNC	[Tp#Ni(μ-CO)$_2$RuCp(D)] (**18′c**)	47
PPh$_3$	[Tp#Ni(μ-CO)$_2$RuCp(D)] (**18′d**)	24
PhC≡CPh	(**19′**)	20

Reactions with soft donors: In contrast to the reactions with hard donors, soft donors (CO, isonitriles, PPh$_3$, Ph−C≡C−H) readily reacted with **3′** to give the corresponding diamagnetic adducts **18′** and **19′** (Table 5).[33]

IR spectra of **18′a–c** and **19′** contain ν_{BH} absorptions above 2500 cm^{-1} indicative of a κ^3-Tp# ligand, whereas the PPh$_3$-adduct **18′d** shows the ν_{BH} band at 2472 cm^{-1}, which is indicative of a κ^2-Tp# ligand.[20] The changes of the ν_{CO} patterns, that is, 1) appearance of $\nu(\mu$-CO) vibrations and 2) replacement of the $\nu(\eta^1$-CO) vibrations by the bands characteristic of the added donors (e.g., ν_{CN} for isonitriles), reveal coordination of the donors to the Ru center, because [(D)$_n$Tp#Ni−RuCp(η^1-CO)$_2$] resulting from coordination to the Ni center is not consistent with these IR features. The CN−R (**18′b,c**) and vinylidene complexes (**19′**) show the CN and C=C stretching vibrations around 2150 and 1550 cm^{-1}, respectively. The functional groups are also characterized by ^{13}C or ^{31}P NMR [δ_C(CN−R) = 140–160 ppm (**18′b,c**);[34] δ_C(>C=C) = 251.8 ppm (**19′**);[35] δ_P(PPh$_3$) = 46.5 ppm (**18′d**)].

R	20′	18′
Cy	**20′b** (24 %)	**18′b** (23 %)
Ph	**20′e** (58 %)	**18′e** (54 %)

Scheme 3.

is associated not only with C=S bond cleavage,[36] but also with oxidation of the metal centers in **20′** ([Tp#NiII–μ-S₂CNR–RuIICp(CO)₂]; cf. [Tp#NiI–RuICp(CO)₂] (**3′**)). A plausible formation mechanism is summarized in Scheme 3. Initial coordination of R–N=C=S to **3′** should form the N-coordinated intermediate. The coordination makes the central carbon atom of the coordinated R–N=C=S more electrophilic so as to be susceptible to nucleophilic addition of a second molecule of the substrate and form the zwitterionic intermediate. Concomitant R–NC elimination and Ru–S bond formation may release the μ-κ^1(S;Ru):κ^1(N;Ni)-imino-dithiocarbonato intermediate, and subsequent intramolecular S-coordination should furnish **20′**. The released R–NC molecule will be trapped by another molecule of **3′** to give **18′**. While C–S cleavage reaction of S-containing heterocumulenes is known,[36] the present one is a new type of transformation on a transition-metal system.

Discussion

Rational and systematic synthesis of the [Tp^{R}M–M′L$_n$]-type xenophilic complexes: The preparative procedures described herein serve as the first rational and systematic synthetic methods for homo- and heterodinuclear xenophilic complexes, which are in sharp contrast to the previous unpredictable and accidental redox disproportionation reactions described in the Introduction.[3] The modified synthesis of the diiron complex **A2** through the reaction of FeCl₂·1.5THF with Na₂Fe(CO)₄ in the presence of pyridine was the only example that did not involve a redox process.[3g]

Notable features of the present system (**1–3′**) are as follows.

1) Xenophilic complexes containing a Tp^R ligand are prepared by the two methods. Direct metalation of a halide precursor is viable, when the Tp^R ligand is less bulky (e.g., Tp#). On the other hand, cationic activation of the Tp^{R}M fragment is essential for a bulky ligand system (e.g., Tp^{iPr_2}). A less bulky Tp^R ligand, however, is associated with another problem in preparation of the halo precursor, [Tp^{R}M–X].[37] While [Tp^{R}M–X] (Tp^R: bulky) is readily obtained by reaction of a Tp^R anion with MX₂, similar reaction of a less bulky Tp^R anion (e.g., Tp#) frequently produces the sandwich adduct [M(Tp^R)₂], which is inert toward subsequent nucleophilic functionalization.

2) The carbonyl–metal fragment to be introduced should be of C_3-symmetry with respect to the M–M′ axis so as to fit the C_{3v}-symmetrical, three wedge-shaped spaces made by the three pz^R rings of the Tp^R ligand. It is notable that even the rather bulky RuCp(CO)₂ fragment of pseudo-C_3 symmetry can be introduced, but reaction of the C_{4v}-symmetrical [Mn(CO)₄]⁻ ion gives a different type of product (**5′**) with threefold symmetry (D_{3d}).

3) On the basis of the crystallographic and spectroscopic data the dinuclear complexes thus obtained are concluded to be "xenophilic complexes".

4) The similar stability of the Tp^{iPr_2} and Tp# derivatives indicates that kinetic stabilization by bulky substituents is not essential for the xenophilic complexes **1–3′**.

5) Tp^R ligands are regarded as equivalents for cyclopentadienyls (η^5-C₅R₅), because both are mono-negative six-electron donors.[7] As for transition-metal organometallics, although many isoelectronic coordinatively saturated complexes containing Tp^R and η^5-C₅R₅ ligands are known, coordinatively unsaturated, low-coordinate [(η^5-C₅R₅)M–X] species are very few and, in many cases, kinetic stabilization by bulky R substituents is essential.[38] In contrast to the η^5-C₅R₅ system, kinetic stabilization is not always essential for coordinatively unsaturated organometallics with a Tp^R ligand, as observed for the present dinuclear complexes as well as the hydrocarbyl complexes.[8] The difference could be interpreted in terms of ligand-field splitting. The N-based Tp^R ligand causes a small ligand-field splitting, which leads to a high-spin electronic configuration with all frontier orbitals being occupied either by electron pairs or by unpaired electrons (see below), whereas the C-based η^5-C₅R₅ ligand causes a large splitting, which leads to a low-spin species with vacant frontier orbital(s) that should undergo further reactions including decomposition.
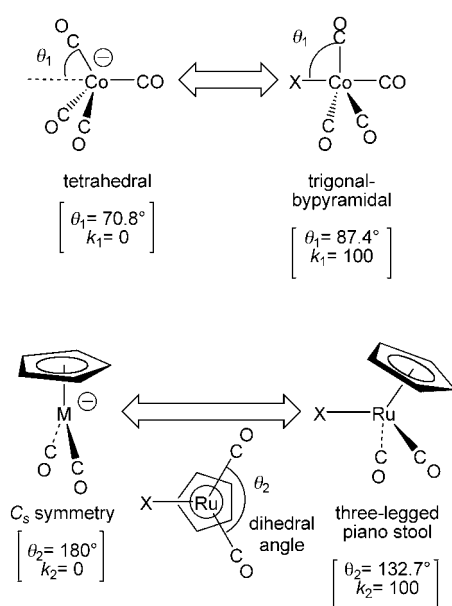
Properties of the metal–metal bond in the xenophilic complexes: The metal–metal bond in the xenophilic complexes **1--3′** is expected to be polarized. Their properties will be discussed by comparing their structural and spectroscopic features with those of reference complexes with and without a covalent M–X bond.

For the Co(CO)₄ complexes **1**, alkylcobalt complex ([R–Co(CO)₄]; R=phthalimodoylmethyl)[39a] and [Co₂(CO)₈][16a, 17] were selected as references for the covalently bonded structure, and [Co(CO)₄]⁻ was chosen as a reference for the ionic structure. The X–Co, Co–CO, and C–O distances and ν_{CO} values for the xenophilic complexes and the references are summarized in Table 6. The extent of the covalent X–M interaction in [X–M′L$_n$] can also be estimated from a structural parameter for the M′L$_n$ part (Scheme 4). As for [X-Co(CO)₃(L)] type complexes, as covalent X–M bonding interaction increases, the structure of the Co moiety changes from a tetrahedral one to a trigonal-bipyramidal one.[40] The distortion can be estimated by the X-Co-CO(equatorial) angle θ_1 (averaged values; Table 6). The structural and vibrational data for **1^{Co}/1′^{Co}** are between those of the two references (Co–CO, θ_1 and ν_{CO}: [R–Co(CO)₄]>**1^{Co}/1′^{Co}**>[Co(CO)₄]⁻; C–O: [R–Co(CO)₄]<**1^{Co}/1′^{Co}**<[Co(CO)₄]⁻), and the xenophilic complexes **1^{Co}**, **1′^{Co}**, and **A1** show very similar characteristics. These features reveal development of substantial negative charge on the Co(CO)₄ fragment in **1^{Co}/1′^{Co}** with respect to the covalent species. When the θ_1 values are normalized according to the

Table 6. Comparison of structural parameters and ν(CO) values of [X−Co(CO)4] species.[a]

[X−Co(CO)4]	X	X−Co	Co−CO_eq	C−O_eq	Co−CO_ax	C−O_ax	θ1 (k1)	ν(CO)	M−X
[R−Co(CO)4][b]	phthalimidoyl-methyl	2.075(3)	1.802	1.133	1.818(4)	1.126(4)	87.4 (100)	2107, 2040, 2029, 2020[b]	covalent
[Co2(CO)8][c]	Co(CO)4	2.522	[c]	–	–	–	–	2069, 2042, 2022[d]	covalent
[(tBuO)3Ti−Co(CO)4][e]	Ti(OtBu)3	2.565(2)	1.75	1.17	1.77(1)	1.17(1)	79.5 (52)	2062, 1998, 1962[e]	ELHB
[Tp^{iPr2}Co−Co(CO)4] (**1^Co**)[f]	CoTp^{iPr2}	2.4696(8)	1.764	1.153	1.793(5)	1.138(6)	77.9 (43)	2052, 1979, 1946[f]	xenophilic
[Tp^#Co−Co(CO)4] (**1'^Co**)[f]	CoTp^#	2.4467(9)	1.777	1.139	1.77(3)	1.13(1)	78.8 (48)	2056, 1987, 1947[f]	xenophilic
[(py)3Co−Co(CO)4]+ (**A1**)[g]	[Co(py)3]+	2.490(2)	1.74	1.14[l]	1.816(13)	1.121	77.9 (43)	2050, 1992, 1943, 1933[g]	xenophilic
[Co(CO)4]−[h]	none	–	1.745	1.156	–	–	70.8 (0)	1880[h]	ionic

[a] Distances in Å and ν(CO) in cm^{-1}. Structural parameters for CO_eq are averaged values. For θ1, θ2, k1, and k2, see the text. [b] Reference [39a]. IR in hexane/toluene. [c] References [16a, 17]. An isomer with bridging CO ligands [(OC)3Co(μ-CO)2Co(CO)3] was characterized by X-ray crystallography. [d] In hexane. [e] Reference [39b]. IR in toluene. [f] Present study. IR in CH2Cl2. [g] Reference [3b]. IR as KBr disk. [h] Structural data for **8'^Ni** and IR data for the PPN salt. IR in THF.

Scheme 4.

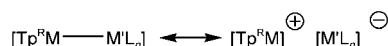the two cp-M-CO planes (θ2; cp: the centroid of a Cp ring; Scheme 4 and Table 8). The ionic species, [MCp(CO)2]−, should have a C_s structure (θ2 = 180), whereas a covalent species should assume a three-legged piano stool structure. Because the structure of [RuCp(CO)2]− is not reported, that of the Fe analogue, K[FeCp(CO)2],[41] was considered instead. Trends similar to the [Co(CO)3(L)] complexes are noted (Ru−CO: [R−RuCp(CO)2] > **3'**; C−O: [R−RuCp(CO)2] < **3'**; θ2: [R−RuCp(CO)2] < **3'** < [MCp(CO)2]−). The k2 value for **3'** is 62. (The k2 values are normalized with respect to [R−RuCp(CO)2] (R = Cp(CO)2RuCH2CH2; k2 = 100) and [MCp(CO)2]− (k2 = 0).)

These structural and IR data reveal development of substantial negative charge on the M'L_n part, in other words, the metal–metal bond in the xenophilic complexes is polarized to a significant extent (Scheme 5). Whittlesey referred

Scheme 5.

two reference structures [k1: 0([Co(CO)4]−)−100([R−Co(CO)4])], k1 values for the xenophilic complexes fall in the range between 40 and 50.

Similar trends were suggested for **A3** by Whittlesey[3g] and are also evident for the [Co(CO)3(PPh3)] derivative **2** (Table 7). The parameters for the xenophilic complex **2^Co** fall between those for the covalently bonded species ([R−Co(CO)3(PPh3)] and [{Co(CO)3(PAr3)}2]) and the ionic species (PPN[Co(CO)3(PPh2OMe)]).

For the [X−RuCp(CO)2] system, covalent and ionic structures may be characterized by the dihedral angles made by

to a shift of ν_{CO} vibrations to lower frequencies and a short M−M distance as diagnostic for xenophilic complexes.[3a,f,g] A substantial shortening of the Co−Co bond lengths in **1^Co** and **2^Co** relative to that in [Co(CO)3(PAr3)]2 (by ca. 0.3 Å) should result from electrostatic attraction of the oppositely charged metal centers. This argument is also supported by 1) the Co−Co distances of **2^Co** (with the more negatively charged Co(CO)3L part) and **1'^Co** (with the more positively charged NiTp^R part) being slightly shorter than that in **1^Co** (by 0.02–0.05 Å) and 2) the DFT calculations described below.

Table 7. Comparison of structural parameters and ν(CO) values of [X−Co(CO)3(PPh3)] species.[a]

[X−Co(CO)3(PR3)]	X	X−Co	Co−CO_eq	C−O_eq	Co−P	θ1 (k1)	ν(CO)	M−X
[R−Co(CO)3(PPh3)][b]	p-tBu-benzyl	2.120(4)	1.779	1.139	2.2497(13)	87.2 (98)	2049, 1983, 1957[b]	covalent
[{Co(CO)3(PAr3)}2][c]	Co(CO)3(PAr3)	2.702(2)	1.788	1.155	2.218(2)	85.0 (86)	1977, 1957[c]	covalent
[Tp^{iPr2}Co−Co(CO)3(PPh3)] (**2^Co**)[d]	CoTp^{iPr2}	2.4234(7)	1.763	1.172	2.194(1)	78.8 (48)	1978, 1954, 1905, 1889[d]	xenophilic
PPN[Co(CO)3(PPh2OMe)][e]	none	–	1.732	1.167	2.127(2)	74.2 (−)	1943, 1847[e]	ionic

[a] Distances in Å and ν(CO) in cm^{-1}. Structural parameters for CO_eq are averaged values. For θ1, θ2, k1, and k2, see the text. [b] Reference [39c]. IR in hexane. [c] PAr3 = PPh2(C6H4-o-CH2NMe2) derivative, reference [39c]. IR in CHCl3. [d] Present study. IR in CH2Cl2. [e] Reference [39d]. IR in MeCN.

Table 8. Comparison of structural parameters and $\nu(CO)$ values of [X−RuCp(CO)$_2$] species.[a]

[X−RuCp(CO)$_2$]	X	X−Ru	Ru−CO	C−O	θ_2 (k_2)	$\nu(CO)$	M−X
(μ-CH$_2$CH$_2$)[RuCp(CO)$_2$]$_2$[b]	CH$_2$CH$_2$RuCp(CO)$_2$	2.189(3)	1.88	1.12	132.7 (100)	2077, 1953 [c]	covalent
[{RuCp(CO)$_2$}$_2$] (**D**)[d]	RuCp(CO)$_2$	2.791(2)	1.81	1.15	133.3 (99)	2018, 1959 [c]	covalent
[(thf)Cp$_2$Lu−RuCp(CO)$_2$][e]	LuCp$_2$(thf)	2.955(2)	1.84	1.16	148.9 (66)	2027, 1965[f]	ELHB
[Tp$^\#$Ni−RuCp(CO)$_2$] (**3′**)[g]	NiTp$^\#$	2.512(1)	1.855	1.16	150.6 (62)	1953, 1891 [g]	xenophilic
K[RuCp(CO)$_2$]	none	–	–	–	180 (0)[h]	1896, 1811[f]	ionic

[a] Distances in Å and $\nu(CO)$ in cm^{-1}. Structural parameters for CO$_{eq}$ are averaged values. For θ_1, θ_2, k_1, and k_2, see the text. [b] Reference [39e]. [c] In hexane. [d] The isomer without μ-CO ligands, reference [32]. [e] Reference [39f]. [f] In THF. [g] Present study. IR as KBr disk. [h] For K[FeCp(CO)$_2$], reference [41].

Comparison with early–late heterobimetallic (ELHB) complexes provides interesting insights into the electronic structures of the metal–metal bonds. The structural parameters including the θ_1/θ_2 values for the M′L$_n$ moieties in [(tBuO)$_3$Ti−Co(CO)$_4$][39b] and [Cp$_2$(thf)Lu−RuCp(CO)$_2$][39f] (Table 6) are comparable to those of the corresponding xenophilic complexes **1^{Co}/1′^{Co}** and **3′**, respectively. But the ν_{CO} vibrations for the ELHB complexes appear in a higher energy region. The most intense ν_{CO} band of [(tBuO)$_3$Ti−Co(CO)$_4$] (1962 cm^{-1}) is higher in energy than that of **1^{Co}** (1946 cm^{-1}) by approximately 15 cm^{-1} and, in particular, the ν_{CO} vibrations of [Cp$_2$(thf)Lu−RuCp(CO)$_2$] are much higher than those of **3′** and are comparable to those of covalent species, indicating a metal–metal interaction with more covalent character for ELHB complexes. These IR data suggest different electronic structures for the metal–metal interactions in the xenophilic complexes and dinuclear complexes with a covalent metal–metal bond such as ELHB complexes.

DFT analysis of xenophilic complexes:[42] To elucidate the electronic structures of the paramagnetic xenophilic complexes unrestricted DFT calculations were performed for the model nickel complexes bearing a simplified Tp^{H_2} ligand,[9] [Tp^{H_2}Ni−Co(CO)$_4$] (**E**), [Tp^{H_2}Ni−Co(CO)$_3$(PH$_3$)] (**F**), and [Tp^{H_2}Ni−RuCp(CO)$_2$] (**G**). The standard complex **E** with singlet and triplet configurations was subjected to geometry optimization and MO calculation. As a result, the triplet species gave a solution of lower energy in accord with the magnetic susceptibility of **1^{Ni}/1′^{Ni}**. The singlet species (**E′**: see below) was distorted and higher in energy than **E** by 34.4 kcal mol^{-1}. Then the other model complexes **F** and **G** were also examined with triplet configurations on the basis of the magnetic susceptibility of **2^{Ni}/2′^{Ni}** and **3′**. The results are summarized in the Supporting Information (SI 2–8[13]). The optimized structures for the triplet species are in good agreement with the structures determined by X-ray crystallography, as compared in the Supporting Information (SI 2[13]). The substitution of the alkyl and bromo groups on the Tp^R ligand by hydrogen atoms (Tp^{H_2}) does not affect the overall structures. The differences in bond lengths are less than 0.1 Å, mostly less than 0.05 Å, which are comparable to the magnitude of substituent effects. For example, replacement of the Tp^{iPr_2} ligand in **1^{Ni}** by the Tp$^\#$ ligand (**1′^{Ni}**) causes shortening of the Ni−Co distance by 0.045 Å as de-

termined by X-ray crystallography (Table 2). The following discussion will focus on the triplet species.

Tp^{H_2}Ni−Co(CO)$_4$ (**E**): Geometry optimization and MO calculations were performed under two conditions: within C_3 symmetry and without any geometrical constraint (C_1 symmetry). The results of the calculations under the former condition will be discussed in more detail and are given in the Supporting Information (SI 2 and 3[13]), because 1) the calculation within C_3 symmetry gave a structure of a lower energy, 2) an essentially C_3 symmetrical structure was obtained even under the C_1 conditions, and 3) the structures of **1^{Ni}** and **1′^{Ni}** are virtually C_3 symmetrical as described above. In addition, a symmetric structure makes analysis of orbital interactions easier.

An MO diagram for **E** is shown in Figure 3 together with those of **F** and **G**. The energy levels for metal-based orbitals and metal–ligand mixed orbitals are indicated with bold lines and normal lines, respectively. The dotted lines are for ligand-based orbitals and many of them are omitted for the clarity. The metal-based orbitals are shown in Figure 4.[43]

Orbitals up to α102 and β100 are filled with unpaired electrons leading to a 202 electron system. The twenty metal-based orbitals shown in Figure 4 are divided into the Co(CO)$_4$-based orbitals (α102–100,95,94, β100–98,93,92) and the NiTp^{H_2}-based orbitals (α88–86,64,63, β102,101,89–87). It is notable that eight pairs of orbitals (α102-β100, α101-β99, α100-β98, α95-β93, α94-β92, α88-β88, α87-β89, α86-β87) are very similar in their energies and shapes. From a simplified MO viewpoint, this electronic configuration corresponds to the situation in which all cobalt d orbitals and a part of the Ni d orbitals (α88-β88, α87-β89, α86-β87) are occupied by electron pairs. In sharp contrast to these orbitals, the other Ni-based orbitals (α64,63, β102,101) are different in energy by about 10 eV, but very similar in their shapes. Because the α64,63 orbitals are filled and the β102,101 orbitals are vacant, the two unpaired electrons on α64,63 lead to the triplet electronic configuration. The large energy separation between the α64,63 and β102,101 orbitals should be due to Coulombic repulsion of the d electrons. Thus this MO picture is in good agreement with the xenophilic structure consisting of the coordinatively saturated Co(CO)$_4$ fragment and the NiTp^R fragment with a high-spin (triplet) electronic configuration. Figure 3 clearly shows that all frontier orbitals are occupied by electrons, and the stability of the coordina-
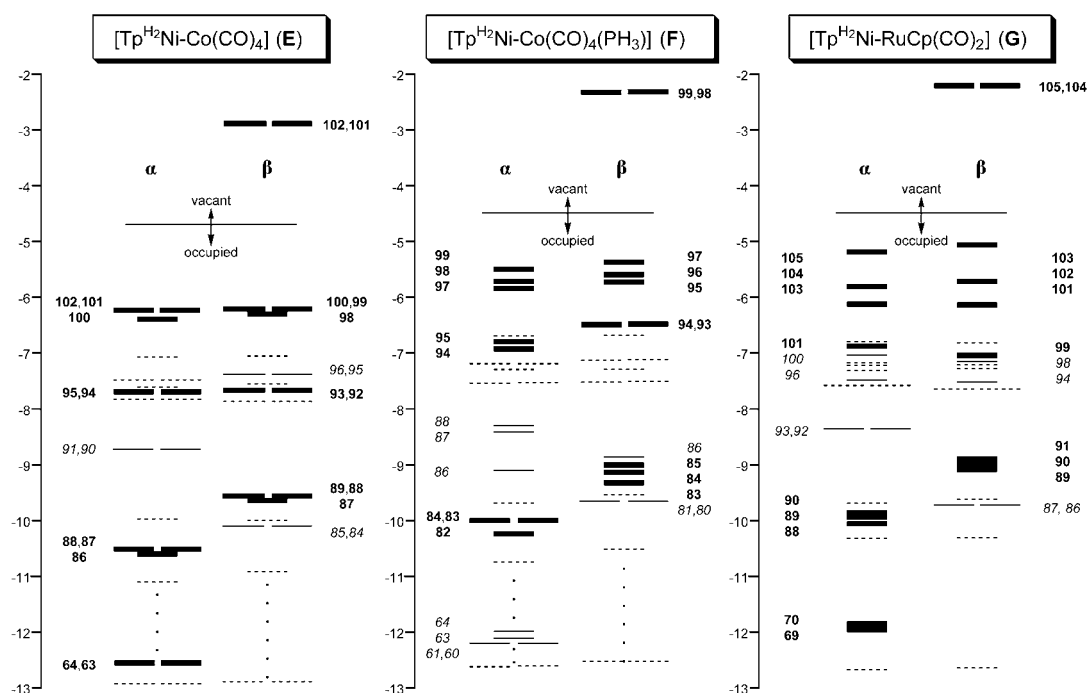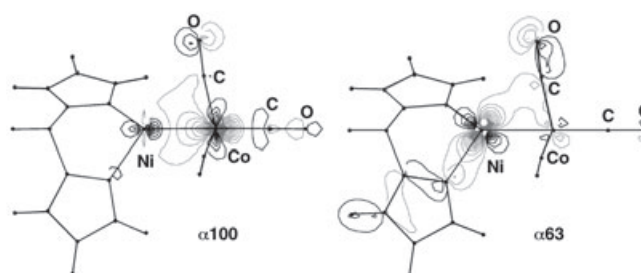
Figure 3. MO diagrams for $[Tp^{H_2}Ni-ML_n]$ $[ML_n = Co(CO)_4$ (**E**), $Co(CO)_3(PH_3)$ (**F**) and $RuCp(CO)_2$ (**G**)]. Bold, normal, and dotted lines are for metal-based orbitals, metal–ligand mixed orbitals, and ligand-based orbitals, respectively.

tively unsaturated species **E** should be ascribed to the lack of a vacant frontier orbital. This type of stabilization of an electron-deficient species is regarded as "spin block", although such a phenomenon is still a matter of debate.[44]

Of the twenty metal-based orbitals, four d_{z^2}-type orbitals ($\alpha100$, $\beta98$, $\alpha86$, and $\beta87$; Ni−Co axis: z axis) are responsible for a M−M σ interaction. While, in these orbitals, contribution of one of the two metal d_{z^2}-type orbitals is predominant (Co: $\alpha100$, $\beta98$; Ni: $\alpha86$, $\beta87$), the orbitals $\alpha100$ and $\beta98$ with out-of-phase combinations take part in anti-bonding M−M σ-interactions and orbitals $\alpha86$ and $\beta87$ with in-phase combination take part in bonding M−M σ-interactions. Accommodation of four electrons in these four orbitals leads to virtually zero bond order for the Ni−Co σ interactions, indicating that covalent σ-bonding interactions are virtually negligible. Very weak $d\pi$–$d\pi$ interactions are found for $\alpha95,94$ and $\beta93,92$, but they are based on anti-bonding combinations.

Slight bending of the Co-C-O(equatorial) linkages from linear structures (~174°) could be related to attractive interaction between the Ni center and the CO carbon atoms, in which the electron density is increased by the action of the negatively charged Co center. The bending is observed irrespective of X in [X−Co(CO)$_4$]. The orbital interaction dominating the bending is the in-phase interaction of the d_{z^2} orbital-like lone pair electrons (or the Co−C σ-bonding electrons in the case of **I**) with p orbitals of the carbon atoms of the equatorial CO ligands, as indicated by the contour plot for $\alpha100$ of **E** (shown here).[43]

However, this back-donating interaction from the Co center to the equatorial CO ligands is anti-bonding in char-

acter with respect to the Ni···CO interaction. Ni···CO attractive interactions are found for $\alpha64,63$, which should contribute not only to the bending but also to connection of the two metal fragments. A contour plot of $\alpha63$ is shown above. However, because 1) the Ni···CO interaction is very weak and 2) very weak anti-bonding counterparts are also found for metal–ligand mixed orbitals with energy around -11.5 eV, the net Ni···CO bonding effect is not significant.

An attractive interaction between the two metal centers, alternative to the covalent interaction, is an electrostatic one between the positively charged NiTp^{H_2} fragment and the negatively charged Co(CO)$_4$ fragment. To evaluate the ionic interaction, comparison is made with the putative complex [Li···Co(CO)$_4$] (**H**; SI 6[13]), in which the lithium cation interacts with the cobalt center. (In the actual Li salt of [Co(CO)$_4$]$^-$, the Li cation weakly interacts with the oxygen atom of the CO ligand, [Li···OC−Co(CO)$_3$].[45]) Comparison is also made with the methyl cobalt complex, [CH$_3$−Co(CO)$_4$] (**I**), a reference compound with a covalent X−Co

[Tp^{H_2}Ni-Co(CO)_4] (E)

vacant

β102   β101

α102   α101   β100   β99

α100   occupied   β98

α95   α94   β93   β92
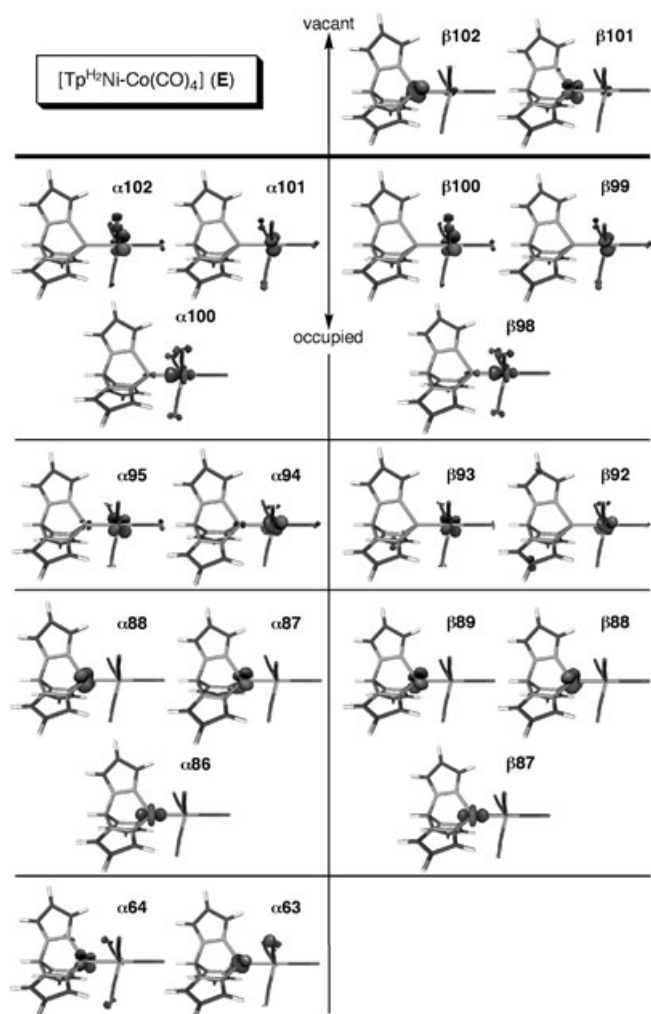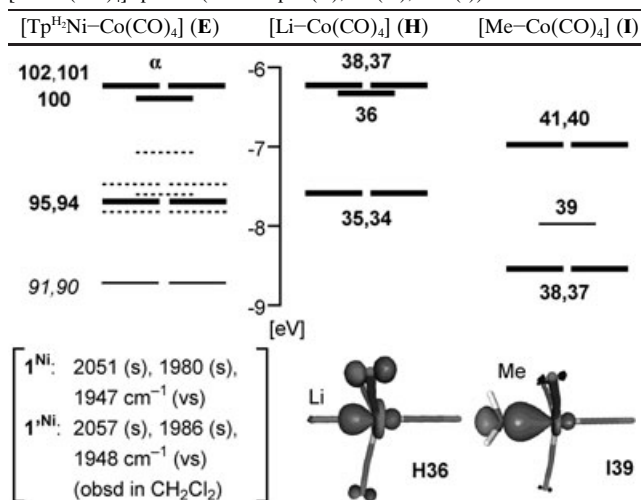
α88   α87   β89   β88

α86   β87

α64   α63

Figure 4. Metal-based molecular orbitals of **E**.

bond (SI 7[13]). The results are summarized in Table 9;[43] for the simplicity only α spin orbitals are shown for **E**.

The Li···Co separation (2.284 Å) is slightly shorter than the sum of covalent radii of Li and Co (2.39 Å = 1.23 + 1.16). At a first glance, the Co-based d orbitals of **E** (**E** 102–100, 95,94) and **H** (**H** 38–34) are very similar in the energy levels and the shapes, but the Co d-orbital levels of **I** are substantially lower in energy than those of **E** and **H**. In particular, the d_{z^2}-type orbital of the covalent species **I** (**I** 39) (CH_3–Co axis: z axis) is strongly stabilized relative to the corresponding orbitals (**E** α100 and **H** 36) owing to the covalent Co–CH_3 interaction, while the energy gaps between the d_{xy} and $d_{x^2-y^2}$ orbitals and the d_{xz} and d_{yz} orbitals are comparable (**H** 38,37–**H** 35,34: 1.36 eV; **I** 41,40–**I** 38,37: 1.53 eV). These data clearly indicate that the metal–metal interaction in **E** resembles the electrostatic Li^{δ+}···Co^{δ-} interaction in **H** rather than the covalent bond in **I**. Furthermore such an interaction is supported by the total atomic charges on Ni (0.840) and Co (−0.386) in **E**.

Results of frequency analysis of the CO stretchings are also shown in Table 9. First of all, the values calculated for

Table 9. Comparison of the features of occupied molecular orbitals of [X–Co(CO)_4] species (X = NiTp^{H_2} (**E**), Li (**H**), Me (**I**)).

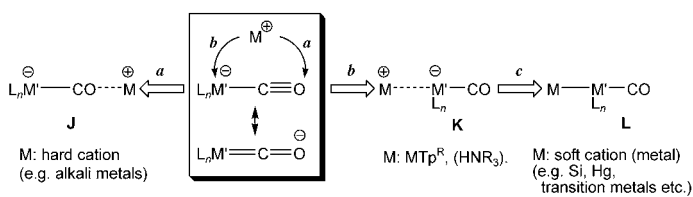| [Tp^{H_2}Ni–Co(CO)_4] (**E**)	[Li–Co(CO)_4] (**H**)	[Me–Co(CO)_4] (**I**)
102,101 100 α −6 38,37		
	36	41,40 (−7)
95,94		39 (−8)
91,90	35,34	38,37 (−9)

[eV]

1^{Ni}: 2051 (s), 1980 (s), 1947 cm^{-1} (vs)
1'^{Ni}: 2057 (s), 1986 (s), 1948 cm^{-1} (vs)
(obsd in CH_2Cl_2)

Li   Me

H36   I39

ν(CO) vibrations [cm^{-1}] (intensity)

2034.6 (497)	2035.4 (317)	2080.3 (165)
1985.5 (378)	1978.0 (364)	2038.6 (362)
1950.4 (887)	1943.3 (1046)	2021.7 (800)
1950.3 (889)	1942.8 (1047)	2021.6 (800)

E are in good agreement with those observed for 1^{Ni} and 1'^{Ni}. In addition, when the CO vibrations of **E** are compared with those of the references **H** and **I**, 1) the ν_{CO} patterns for **E** and **H** are very similar with each other and 2) the CO vibrations of **I** are shifted to higher frequencies by approximately 50 cm^{-1}, due to a decreased back-donation that results from localization of Co d electrons onto the covalent Co–CH_3 bond.

Thus the present DFT calculation leads to a conclusion that the interaction between the two metal centers in [Tp^{H_2}Ni–Co(CO)_4] (**E**) is not so covalent as in [CH_3–Co(CO)_4] (**I**), but is as ionic as in [LiCo(CO)_4] (**H**). The virtually negligible covalent interaction is supported by the constant ν_{CO} vibrations and the isostructural features for a certain series of [Tp^{R}M–Co(CO)_3(L)]-type complexes irrespective of M.

Two modes are feasible for interaction of carbonylmetalates with a cation, that is, oxygen- (**J**) and metal-atom interactions (**K**; Scheme 6), because the anionic charge is delocalized over the M-C-O linkage. In principle, hard and soft cationic species would form O- and M-interacting structures, respectively. In the case of the interaction of [Co(CO)_4]^-

L_nM'—CO····M   a   L_nM'—C≡O   b   M····M'—CO   c   M—M'—CO
                                          L_n   L_n   L_n
J   L_nM'=C=O   K   L

M: hard cation   M: MTp^R, (HNR_3).   M: soft cation (metal)
(e.g. alkali metals)   (e.g. Si, Hg,
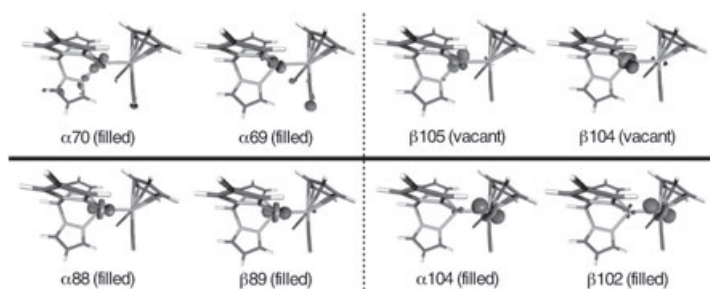   transition metals etc.)

Scheme 6.

with alkali metals, which are typical hard cations, the O interaction (**J**) has been confirmed by X-ray crystallography,[45] whereas interaction with soft metal fragments is not terminated at the stage of **K**, but further leads to a covalent species (**L**). To the best of our knowledge, no Co-interacting ionic species (**K**) has been reported so far. Trialkylammonium salts, [$R_3NH\cdots Co(CO)_4$],[46] may be the most relevant system, but they are not ionic species; rather they are hybrids of ammonium cobaltate and an amine adduct of hydride [$R_3N\cdots HCo(CO)_4$].

The Tp^R complexes **1/1′** (**E**) and **A1** (Scheme 1) are regarded as tetracarbonylcobaltates, in which the cation interacts with the cobalt center (**K**; Scheme 6). It should be noted that the M–M distances in the ionic species **1/1′** and **A1** are substantially shorter than the covalent M–M bond. While the ionic picture of the metal–metal interaction was suggested previously,[3a,g] the present study verifies the predominant electrostatic interaction on the basis of the unrestricted DFT calculations. In accord with such an ionic interaction, the metal–metal interaction in **1/1′** and **2/2′** is readily cleaved in a polar medium such as MeCN as described above. Although structural drawings with a bond between the two metal centers may not be correct, such expressions are used for the sake of convenience.

*[Tp^{H_2}Ni–Co(CO)$_3$(PH$_3$)] (**F**)*: For the PH$_3$-substituted derivative **F**, structure optimization was carried out without geometrical constraint to examine the bending of the Ni-Co-P linkage. As a result, an MO diagram very similar to that of **E** is obtained (Figure 3; SI 4[13]), although the calculation with no geometrical constraint causes mixing of the metal- and ligand-based orbitals as well as separation of the degenerate orbitals. All the cobalt d orbitals (α99–97,95,94, β97–93) and a part of the Ni orbitals (α84–82 and β85–83) are occupied by electron pairs, whereas accommodation of each one electron in α64,63 leads to a triplet configuration (cf. β99,98: vacant).

The bending of the Ni-Co-P linkage (172.7°; cf. **2^{Ni}**: 172.23(7)°, **2′^{Ni}**: 160.06(6)°) can be interpreted in terms of orbital interactions found in **F** α64,63, which are essentially the same as those in **E** α64,63 (responsible for the weak O$\rightarrow$ Ni donating interaction). Replacement by the PPh$_3$ ligand increases the electron density at the Co center to promote back-donation to the CO ligands, which further enhances the donating interaction from the CO ligands to Ni. The donating interaction should become much more effective by approach of the CO carbon atom to the Ni center (i.e. folding of the Ni-Co-CO(equatorial) angle), which consequently brings about bending of the Ni-Co-L(axial) linkage. Although such a bending causes a loss in the similar donating interactions from the other two equatorial CO ligands to Ni, the effective interaction with the more folded CO ligand would compensate the loss. However, the Ni$\cdots$CO interaction is so weak as to be fluxional, because the three pyrazolyl rings are equivalent at RT, as observed by ^{1}H NMR spectroscopy (methyl signals for the pz$^\#$ groups of **2′^{Ni}**: $\delta_H = 2.1$ (9H), -7.1 ppm (9H)).

*[Tp^{H_2}Ni–RuCp(CO)$_2$] (**G**)*: Structure optimization of **G** was carried out under no geometrical constraint. The MO diagram for the resultant virtually C_s symmetrical structure **G** (Figure 3; SI 5[13]) consists of orbital interactions similar to those of **E** and **F**, although, of course, orbitals of different characters arising from the RuCp(CO)$_2$ fragment are included. All Ru-based d orbitals (α105–103,101,96, β103–101,99,94) and a part of the Ni-based orbitals (α90–88, β91–89) have their counterparts of similar energies and shapes to form pairs of orbitals as noted for **E**, whereas the Ni-based orbitals (α70,69) do not have their counterparts in the similar energy region and, instead, the Ni-based orbitals of β-spin (β105,104) are found in the higher energy region (Figure 3). The shapes of the two pairs of orbitals, α70-β105 and α69-β104 (shown here), are similar as also noted for **E** and **F**. Accommodation of 208 electrons leaves the higher energy orbitals (β105,104) vacant to form the triplet electronic configuration with two unpaired electrons on α70,69 on Ni; on the other hand, the RuCp(CO)$_2$ moiety is coordinatively saturated.

α70 (filled) α69 (filled) β105 (vacant) β104 (vacant)

α88 (filled) β89 (filled) α104 (filled) β102 (filled)

The orbitals responsible for the Ru–Ni σ interaction are also shown here.[43] The α88-β89 and α104-β102 orbitals are bonding and anti-bonding orbitals, respectively, and accommodation of four electrons leads to virtually zero Ni–Ru σ-bond order, suggesting that the dinuclear structure is based on ionic interaction between the two metal fragments as concluded for **E**. Let us point out that the shapes and energy levels of the Ni-based orbitals of **G** are very similar to those of the corresponding orbitals of **E** and **F**, that is, the Tp^{H_2}Ni orbitals are not much affected by the organometallic M′L$_n$ fragment, owing to the very weak covalent interaction between the two metal centers.

Divergent reactivity of the xenophilic complexes: The xenophilic complexes **1**, **1′**, and **3′** show divergent reactivity dependent on the properties of the donor molecules to be reacted. Roughly speaking, hard nucleophiles (N- and O-donors) attack the Tp^{R}M moiety, in the case of **1/1′**, to give the ion pairs, whereas soft nucleophiles attack the organometallic moiety (e.g.,Co(CO)$_3$(L), RuCp(CO)$_2$) to give the substituted products or addition products. Plausible reaction mechanisms are summarized in Scheme 7, in which mechanisms for the Tp^{R}Ni systems are shown for convenience.
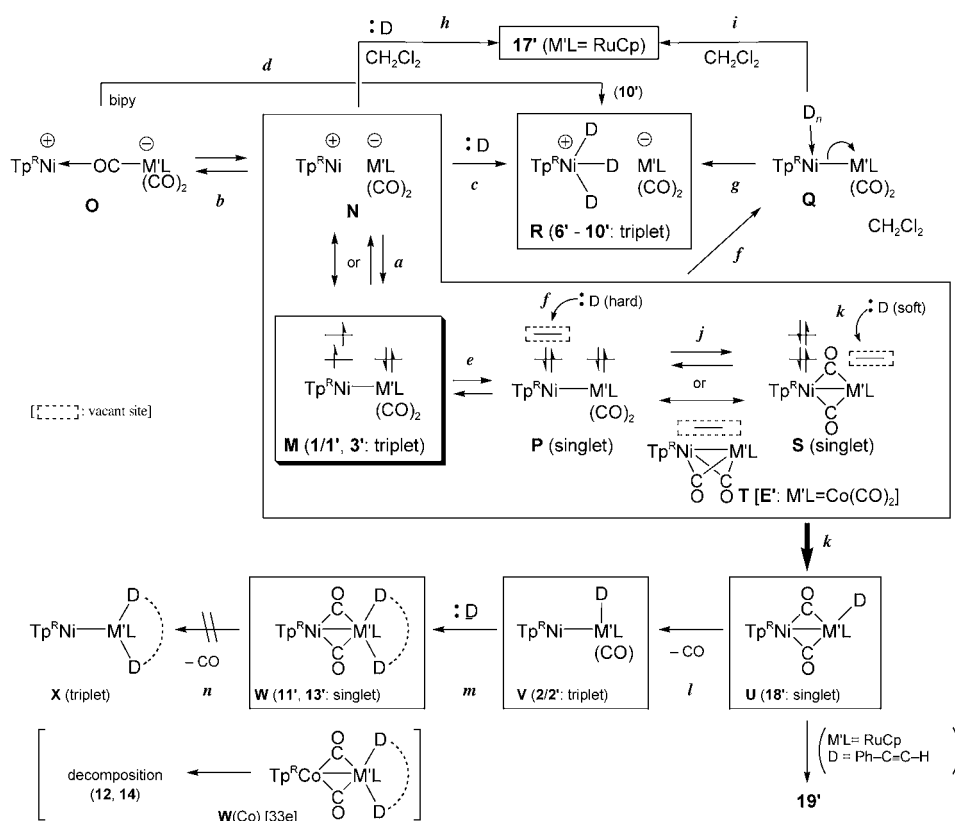
Scheme 7.

Reaction with hard donors: Two mechanisms are plausible for the heterolytic cleavage of the metal–metal interaction in **1/1′** and **2/2′**, which is clear evidence for its polar nature. One involves a spontaneous dissociation equilibrium (step *a*) and the other involves a bond cleavage process induced by interaction with the donor (steps *e–g*).

The former mechanism may be supported by the structure of **10′** (Table 4), which is apparently formed by way of 1) trapping of the ionized form **N** by bipy (step *c*) or 2) coordination of bipy to the μ-isocarbonyl intermediate **O** (step *d*). Although neither **N** nor **O** (steps *a* and *b*) has been detected in non-coordinating solvents (e.g., CH₂Cl₂), this possibility cannot be excluded completely as the DFT calculations suggest the Co-interacting form **N** with a short metal–metal distance as the dominant resonance contributor.

The other mechanism is associated with spin-crossover (step *e*). Metal–metal bond heterolysis is not unique for xenophilic complexes. For example, Geoffroy reported that treatment of [(OC)(Ph₃P)Rh−Co(CO)₄] with MeCN caused Rh−Co bond heterolysis to give the ion pair, [(OC)-(Ph₃P)₂Rh(NCMe)]⁺[Co(CO)₄]⁻, which reverted to the starting complex upon evaporation.[47] The electron-withdrawing Co(CO)₄ part enhances the electrophilicity at the coordinatively unsaturated Rh center, which is susceptible to nucleophilic attack by the donor. Furthermore the [Co(CO)₄]⁻ ion resulting from the heterolysis is stable, and the cationic metal residue is stabilized by coordination of

the donor to furnish the square-planar adduct. The xenophilic complexes **1–3′** are also electron-deficient species, but no vacant frontier orbital for coordination of a donor molecule is available owing to the high-spin configuration. A vacant site, however, could be generated through flipping and pairing of the unpaired electrons in the frontier orbitals, that is, spin-crossover (step *e*). In addition, the adduct formation with soft donors (see below) should also involve an analogous high-spin to low-spin conversion, because the reactants (triplet) and the products (singlet) differ in spin states. Spin crossover is a new idea for understanding the behavior of paramagnetic transition-metal complexes.[48]

The singlet species resulting from the spin-crossover was examined by a DFT calculation. Geometry optimization was performed starting from the optimized structure of **E** (triplet; see above) by simply changing the spin state from triplet to singlet. An optimized structure for the coordinatively unsaturated 32e species (**E′**: singlet; SI 8[13]) and its LUMO are shown here.[43]

The shifting of two of the four CO ligands to the semi-bridging sites leads to a distorted C_s-symmetrical structure. The core structure resembles those of **11′a** and **13**. The
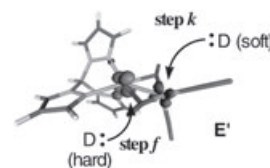
LUMO is developed over the two metal centers with more contribution of the Ni orbital and consists of an anti-bonding π-interaction of the d orbitals of Ni and Co. Therefore donor molecules can interact with either of the metal centers, and coordination of a hard donor to the hard Ni center (step *f*) followed by elimination of [ML(CO)₂]⁻ (step *g*) produces the ion pair **R** when [ML(CO)₂=Co(CO)₄].

These two mechanisms cannot be differentiated by the experimental results obtained so far. An intermediate **N(O)**, **P**, or **T** generated as a very minor component of the equilibria (not enough for a spectroscopic detection) may be trapped by the donor to finally furnish the ion pair **R**.

Reactions involving insertion of organic carbonyl groups ($>C=O$) into a M−M bonds were reported by Gade for ELHB complexes, [LZr−MCp(CO)$_2$] (L = tripodal amido ligand; M = Fe, Ru).[26] While we expected a similar reaction for **1′**, only ligand replacement was observed for the reaction with diphenylcyclopropenone to form **7′** (**R**) (Table 1). Nucleophilic addition of the liberated [Co(CO)$_4$]$^-$ ion to the acyl carbon atom of the coordinated ketone in **7′** would afford an insertion product, but the insufficient electrophilic activation by the MTp$^{\#+}$ fragment as well as the very weak nucleophilic cobaltate may terminate the reaction at the stage of the ionized form **7′** (**R**). The reaction with R-NCS (Scheme 3) is the only indication of an insertion reaction.

Reactions of the Ru−Ni complex **3′** are complicated. Dissolution in polar solvents such as MeCN, acetone, and THF gives intractable mixtures of products, and reaction in CH$_2$Cl$_2$ described above produces mixtures of the chloro complex, [Tp$^{\#}$Ni(D)$_2$−Cl] (**17′**), and [{RuCp(CO)$_2$}$_2$] (**D**), which are apparently formed by means of an unknown radical mechanism. Because **3′** is stable in CH$_2$Cl$_2$, a radical intermediate should be formed upon interaction of **3′** with hard donors [**N** (step *h*) or **Q** (step *i*)]. The different reaction pathways observed for the Co(CO)$_4$ and RuCp(CO)$_2$ complexes should be attributed to the large difference in their acid–base properties, that is, pK_a = 8.3 [H−Co(CO)$_4$] versus 20.2 [H−RuCp(CO)$_2$].[30] The much more stable [Co(CO)$_4$]$^-$ ion, in other words, a good leaving group, should be readily dissociated from the dinuclear entity to give **N** (from **M**) or **R** (from **Q**).

Reaction with soft donors: Reaction of the Co(CO)$_4$ complexes **1/1′** (**M**) with PPh$_3$ results in CO-replacement to give the PPh$_3$ derivative **2/2′** (**U**), whereas the NiTp$^{\#}$ complex **1′^{Ni}** undergoes addition reactions with diphosphines and isonitriles to give the diamagnetic 1:2 adducts (**V**). Reaction of the Ru complex **3′** with soft donors results in coordination to the Ru center to give the adducts **18′** and **19′** (**U**).

First of all, the conversion of the triplet species **1** and **3′** into the singlet products should involve a spin-crossover process (step *e*) to make the conversion spin-allowed. Furthermore, taking into account the structures of the reaction products having bridging CO ligands, the subsequent reaction mechanism should also involve isomerization from a η^1-CO form to a μ-CO form, which is frequently observed for polynuclear carbonyl complexes.[49] The regiochemistry seems to be determined by the soft–hard theory.[50] Soft donors should prefer the soft metal–carbonyl fragment in **S** (in equilibrium with **P**) or the delocalized intermediate **T** (**E′** when M′L = Co(CO)$_2$). While the contribution of the Co orbital to the LUMO in **E′** is less than that of the Ni orbital, the open space over the Co center may make the addition to the Co center kinetically favorable. Addition of a soft donor to the M′ site in **S** or **T** gives the coordinatively saturated 34-electron species (**U**: step *k*). The reactions of **3′** are terminated at this stage, but those of the Co(CO)$_4$ derivatives **1/1′** eliminate a CO ligand to furnish the substituted xenophilic complex **V** (**2/2′**) (step *l*). The robust Ru−CO

bond in **U** (from **3′**) relative to the Co−CO bond in **U** (from **1/1′**) should hinder CO elimination causing the ligand replacement.

In the case of the reactions of **1′^{Ni}** with isonitrile or diphosphine, a repeated nucleophilic addition of the donor to the Co moiety in **V** (steps *l,m*) forms the product **W** with two bridging CO ligands, but further ligand elimination producing a new disubstituted xenophilic complex **X** (step *n*) does not occur.

Another key point of the present addition reactions is the electron counting of the adducts. The adducts **W** formed from the nickel complex **1′^{Ni}** are coordinatively saturated dinuclear species with a 34-electron configuration and, accordingly, the products are stable and diamagnetic. If it is assumed that the reaction pathways for the Ni and Co complexes are similar, the reactions of the Co derivative **1′^{Co}** should form paramagnetic, coordinatively unsaturated 33-electron species **W(Co)**, which should further undergo fragmentation of the dinuclear structure accompanied by redox disproportionation to give the final products without the Tp$^{\#}$ ligand (**12**, **14**).

Conclusion

This paper describes the results of the first systematic study of synthesis, characterization, and chemical properties of a series of xenophilic complexes containing a MTp^R fragment, [Tp^{R}M−M′L$_n$] **1/1′**, **2/2′**, and **3**. It is revealed that 1) their metal–metal bonds are polarized [Tp^{R}M$^{\delta+}$ $^{\delta-}$M′L$_n$], 2) the stability of coordinatively unsaturated xenophilic complexes arises from the lack of a vacant frontier orbital due to a high spin configuration (spin block),[44] 3) the metal–metal σ interaction is not covalent with virtually zero σ-bond order, 4) the two metal centers are held together mainly by electrostatic attraction between the oppositely charged metal fragments, and 5) xenophilic complexes **1–3′** are regarded as carbonylmetalates, in which the cation interacts with the metal center rather than with the hard CO oxygen atom. The simple dinuclear structures of **1–3′** lead to the successful analysis of their electronic structures and chemical properties, and the insights obtained by the present study could be extended to interpretation of the more complicated systems **A** (Scheme 1).

Critical differences between the M−M interactions in xenophilic complexes and polar M−M bonds (e.g., ELHB complexes) can be interpreted in terms of Scheme 8, which illustrates qualitative σ-bonding interactions. The metal–metal bond in homodinuclear complexes is a pure covalent σ bond. Heterodinuclear complexes consisting of different metal fragments contain a covalent bond, but, owing to the different orbital energies, contribution of the lower energy metal component (M) to the M−M′ σ bond is larger than that of the other metal fragment (M′). The resultant electronic structure is best described as a resonance hybrid of the covalent form and the ionized form, in which the M and M′ parts are, to some extent, negatively and positively
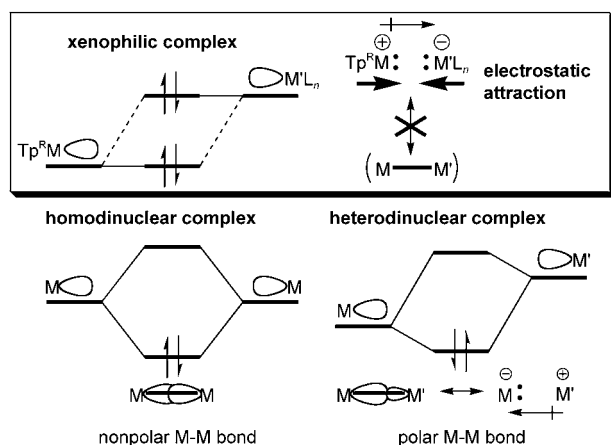
Scheme 8.

charged, respectively. The unequal electron distribution makes the M−M′ bond polar, but the basic interaction is still a covalent interaction, although contribution of the ionic resonance structure is variable depending on the properties of the metal fragments and, in some cases, $d\pi$–$d\pi$ interactions may participate in the bonding interaction. There may be some electrostatic interaction, but it is not so significant as in the case of xenophilic complexes. In contrast to these situations, both bonding and anti-bonding M−M σ-bonding orbitals of the particular $[Tp^R M−ML'_n]$ series of xenophilic complexes are occupied by electron pairs leading to virtually no covalent σ-bonding interactions. Instead electrostatic attraction between the oppositely charged metal centers holds the two metal fragments together. The development of the charges on the two metal fragments does not originate from the σ orbitals, but from electronic configurations of the metal components, which are not associated with the σ interaction. One may be surprised to find that the metal fragment of a higher orbital energy (the $M'L_n$ part) is negatively charged in contrast to heterodinuclear complexes, although, at the moment, we have no idea whether this tendency is a general one or not. The lack of a σ-bonding interaction is strongly supported by 1) no dependence of the ν_{CO} vibrations and the core structures of a certain $[Tp^R M−Co(CO)_3(L)]$ series of complexes on M and 2) the very similar $Tp^{H_2}Ni$-based orbitals in the three molecules (**E**, **F**, and **G**) irrespective of the $M'L_n$ fragments (Figure 3).

Reactions of **1–3′** with hard and soft donors afford products resulting from interaction with the MTp^R and $M'L_n$ parts, respectively. Despite the lack of a vacant site, the xenophilic complexes readily react with singlet donor molecules by means of spin-crossover. The electronic structures of the xenophilic complexes are so flexible that their spin state should be changed to singlet through spin-crossover to render the chemical transformation spin-allowed. The xenophilic species, therefore, can be viewed as a masked form of a reactive, coordinatively unsaturated intermediate. The unique xenophilic complexes described herein should result from the unique coordination properties of the Tp^R ligand, in particular, as a tetrahedral enforcer.[7]

Experimental Section

General methods: All manipulations were carried out under an inert atmosphere by using standard Schlenk tube techniques. THF, diethyl ether, hexanes, toluene (Na-K alloy), CH_2Cl_2, MeCN (P_2O_5), and MeOH (Mg-(OMe)$_2$) were treated with appropriate drying agents, distilled, and stored under argon. ^1H, ^{13}C, and ^{31}P NMR spectra were recorded on JEOL GX-270, Lambda-300, and Lambda-500 spectrometers. Solvents for NMR measurements containing 0.5% TMS were dried over molecular sieves, degassed, distilled under reduced pressure, and stored under Ar. IR spectra were recorded on a JASCO FT/IR 5300 spectrometer as KBr pellets unless otherwise stated and reported in cm^{-1}. Magnetic susceptibility was measured on a Sherwood Scientific MSB-AUTO. $[Tp^{iPr_2}M−Cl]$,[51a] $[Tp^{Ph,Me}M−Cl]$,[51b] $KTp^{\#}$,[51c] $4 \cdot PF_6$,[14] $PPN[Co(CO)_4]$,[21] and $K[RuCp(CO)_2]$[52] were prepared according to the published methods. Preparation of $[Tp^{\#}Ni−Br]$ and $[Tp^{\#}Co−Cl]$ is described in the Supporting Information (SI 9[13]). Other chemicals were purchased and used as received.

Synthesis of 1: As a typical example, the synthetic procedures for 1^{Ni} is described below. Complexes $1^{Mn,Fe,Co}$ were prepared in an analogous manner. CH_2Cl_2 (10 mL) was added to a mixture of $[Tp^{iPr_2}Ni-(NCMe)_3]PF_6$ ($4^{Ni} \cdot PF_6$; 300 mg, 0.379 mmol) and $PPN[Co(CO)_4]$ (403 mg, 0.568 mmol), and the resultant solution was stirred for 2 h at ambient temperature. After removal of the volatiles under reduced pressure the residue was extracted with ether and the deep purple crystal 1^{Ni} (143 mg, 0.206 mmol, 55% yield) was obtained by crystallization at −20 °C.

Data for 1^{Ni}: ^1H NMR (300 MHz, [D$_6$]benzene, 25 °C, TMS): $\delta = 82.43$ (3H), 6.16 (3H), 3.15 (18H), 1.84 (3H), −0.64 (18H), −10.30 ppm (1H); elemental analysis calcd (%) for $C_{31}H_{46}BN_6O_4CoNi$: C 53.56, H 6.67, N 12.09; found: C 53.34, H 6.91, N 12.19.

Data for 1^{Co}: Dark green crystals; ^1H NMR (300 MHz, [D$_6$]benzene, 25 °C, TMS): $\delta = 80.1$ (3H), 8.0 (3H), 3.3 (18H), 2.5 (21H), −25.1 ppm (1H); elemental analysis calcd (%) for $C_{31}H_{46}BN_6O_4Co_2$: C 53.34, H 6.67, N 12.08; found: C 53.48, H 6.68, N 11.77.

Data for 1^{Fe}: Pale green crystals; ^1H NMR (300 MHz, [D$_6$]benzene, 25 °C, TMS): $\delta = 66.9$ (3H), 14.7 (18H), 3.3 (6H), −1.1 (18H), −6.1 ppm (1H); elemental analysis calcd (%) for $C_{31}H_{46}BN_6O_4CoFe$: C 53.78, H 6.70, N 12.14; found: C 53.78, H 6.91, N 10.88.

Data for 1^{Mn}: Pale green crystals; ^1H NMR (300 MHz, [D$_6$]benzene, 25 °C, TMS): $\delta = 80.5$ (3H), 8.0 (6H), 3.3 (18H), 2.5 (18H), −25.3 ppm (1H); elemental analysis calcd (%) for $C_{31}H_{48}O_5N_6BCoMn$ ($1^{Mn} \cdot H_2O$): C 52.48, H 6.82, N 11.85: found: C 52.43, H 7.05, N 11.91.

Synthesis of 1′: As a typical example, the synthetic procedures for $1'^{Ni}$ is described below; $1'^{Co}$ was prepared in an analogous manner. A solution of $KCo(CO)_4$ in THF (10 mL) was prepared by treatment of $[Co_2(CO)_8]$ (100 mg, 0.29 mmol) with $NaK_{2.8}$. $[Tp^{\#}Ni−Br]$ (300 mg, 0.446 mmol) was added to the resultant solution and the mixture was stirred overnight. Extraction with hexane (20 mL), filtration through a Celite pad, removal of the volatiles under reduced pressure and crystallization of the residue from hexane at −20 °C gave $1'^{Ni}$ as dark purple crystals (198 mg, 0.26 mmol, 58% yield).

Data for $1'^{Ni}$: ^1H NMR (300 MHz, [D$_6$]benzene, 25 °C, TMS): $\delta = 4.8$ (9H), −6.9 (9H), −11.4 ppm (1H); elemental analysis calcd (%) for $C_{19}H_{19}O_4N_6BBr_3CoNi$: C 29.89, H 2.51, N 11.21, Br 31.39; found: C 29.82, H 2.81, N 10.96, Br 31.20.

Data for $1'^{Co}$:[53] A very broad ^1H NMR signal (in [D$_6$]benzene) centered around 15 ppm was observed.

Synthesis of 2 and 2′: As a typical example, the synthetic procedures for 2^{Ni} are described below and $2^{Mn,Fe,Co}$ and $2'^{Ni,Co}$ were prepared in an analogous manner. A solution of 1^{Ni} (300 mg, 0.432 mmol) and PPh_3 (113 mg, 0.432 mmol) in toluene (10 mL) was stirred for 3 h at ambient temperature. Filtration through a Celite plug followed by concentration of the filtrate and crystallization from toluene/pentane gave 2^{Ni} as dark red crystals (95 mg, 0.102 mmol, 35% yield).

Data for 2^{Ni}: ^1H NMR (300 MHz, [D$_6$]benzene, 25 °C, TMS): $\delta = 76.8$ (6H), 8.9 (3H), 7.6 (6H), 7.0 (6H), 3.9 (3H), 2.8 (18H), 1.8 (3H), −0.1

FULL PAPER

(18H), −10.9 ppm (1H); elemental analysis calcd (%) for $C_{48}H_{62}BN_6O_3PCoNi$: C 62.33, H 6.62, N 9.04; found: C 61.88, H 6.76, N 8.99.

Data for 2^{Co}: Brown crystal; ^1H NMR (300 MHz, [D_6]benzene, 25°C, TMS): $\delta = 70.5$ (3H), 26.9 (3H), 21.7 (6H), 10.2 (3H), 10.0 (6H), 9.3 (18H), 2.1 (3H), −15.6 (18H), −37.4 ppm (1H); elemental analysis calcd (%) for $C_{51.5}H_{66}BN_6O_3PCo_2$ (2^{Co}·(toluene)$_{0.5}$): C 63.39, H 6.71, N, 8.61; found: C 63.18, H 6.74, N 8.21.

Data for 2^{Fe}: Brown crystals;[53] ^1H NMR (300 MHz, [D_6]benzene, 25°C, TMS): $\delta = 63.2$ (3H), 9.2 (3H), 8.0 (18H), 7.7 (6H), 6.42 (6H), 6.0 (6H), 1.5 (18H), −12.0 ppm (1H).

Data for 2^{Mn}: Brown crystals;[53] ^1H NMR (300 MHz, [D_6]benzene, 25°C, TMS): $\delta = 70.4$ (3H), 26.8 (3H), 21.6 (6H), 10.2 (3H), 10.0 (6H), 9.2 (18H), −12.1 (18H), −37.3 ppm (1H).

Synthesis of 2^{Ni}: A solution of K[Co(CO)$_3$(PPh$_3$)] in THF (10 mL) was prepared by reduction of [Co(CO)$_3$(PPh$_3$)]$_2$ (133 mg, 0.164 mmol)] with Na-K alloy. [Tp$^#$Ni−Br] (200 mg, 0.297 mmol) was added to the resultant solution and the mixture was stirred overnight. Removal of the volatiles under reduced pressure, extraction with toluene (20 mL), filtration through a Celite pad, concentration, and crystallization of the resultant residue from toluene/pentane at −20°C gave 2^{Ni} as deep purple crystals (106 mg, 0.107 mmol, 36% yield). ^1H NMR (300 MHz, [D_6]benzene, 25°C, TMS): $\delta = 8.6$ (6H), 7.5 (3H), 6.9 (3H), 2.1 (9H; pz$^#$), −7.1 (9H; pz$^#$), −12.2 ppm (1H; BH); elemental analysis calcd (%) for $C_{39.5}H_{38}O_3N_6PBBr_3CoNi$ (2^{Ni}·(toluene)$_{0.5}$): C 45.45, H 3.67, N 8.05; found: C 45.67, H 3.70, N 8.08.

Synthesis of $3'$: Sonication of a suspension of [Tp$^#$Ni−Br] (300 mg, 0.446 mmol) and K[RuCp(CO)$_2$] [prepared by reduction of [Ru$_2$Cp$_2$(CO)$_4$] (149 mg, 0.335 mmol) with Na-K alloy in THF and dried in vacuo] in toluene (10 mL) gave a brown precipitate, which was filtered through a Celite pad, evaporated under reduced pressure, and extracted with CH$_2$Cl$_2$. Concentration and crystallization from CH$_2$Cl$_2$/hexane gave $3'$ as dark brown crystals (148 mg, 0.181 mmol, 41% yield). IR: $\nu = 2553$ (BH), 1953 (vs, CO), 1891 cm^{-1} (vs, CO); UV/Vis λ (ε) = 988 (109), 859 (39), 649 (137), 505 (904), 388 nm (1089); ^1H NMR (300 MHz, [D_6]benzene, 25°C, TMS): $\delta = 8.7$ (5H), 1.9 ppm (9H); the other Me signal could not be located; elemental analysis calcd (%) for $C_{24.1}H_{28.8}O_2N_6$-$BBr_3Cl_{0.6}NiRu$ ($3'$·(CH$_2$Cl$_2$)$_{0.3}$·(hexane)$_{0.3}$): C 33.42, H 3.35, N 9.70, Br 27.68, Cl 2.46; found: C 33.05, H 3.50, N 9.34, Br 27.14, Cl 2.41.

Evaporation of the filtrate followed by crystallization from toluene/Et$_2$O gave $16'$. IR: $\tilde{\nu} = 3703$ (w, O−H), 2957 (w, O−H), 2925 (m, O−H), 2856 (w, O−H), 2518 cm^{-1} (m, BH); elemental analysis calcd (%) for $C_{39}H_{55}O_2N_{14}B_2Br_7Ni_2$ (16·Et$_2$O): C 32.30, H 3.82, N 13.52, Br 38.57; found: C 32.30, H 3.82, N 12.89, Br 38.76.

Synthesis of $5'$: [Tp$^#$Ni−Br] (300 mg, 0.045 mmol) was added to a solution of K[Mn(CO)$_5$] in THF [0.05 mmol; generated in situ from NaK$_{2.8}$ and [Mn$_2$(CO)$_{10}$] in THF (10 mL)] and the resultant mixture was stirred overnight. NEt$_4$I (1 equiv) was added to the reaction mixture, which was further stirred overnight. Addition of toluene (10 mL) was followed by removal of the insoluble materials by filtration through a Celite pad. Addition of hexane followed by crystallization at −20°C gave complex $5'$ (48 mg, 0.0028 mmol, 13% yield). IR: $\tilde{\nu} = 3072$ (w, CH), 2959 (m, CH), 2924 (m, CH), 2852 (w, CH), 2537 (m, BH), 1958 (s, CO), 1894 (s, CO), 1847 (vs, CO), 1793 cm^{-1} (v, CO).[53]

Reaction of 1 and $1'$ with hard donors: As a typical example, the synthetic procedures for 6^{Ni} are described below; other complexes were prepared in an analogous manner. Addition of 4-*tert*-butylpyridine (60 μL, 0.485 mmol) to a solution of 1^{Ni} (0.100 g, 0.131 mmol) in CH$_2$Cl$_2$ (10 mL) caused a color change to green. After the mixture was stirred for 1 h the volatiles were removed under reduced pressure and the residue was crystallized from THF/hexane to give 6^{Ni} as blue crystals (119 mg, 0.102 mmol, 78% yield).

Data for 6^{Ni}: IR: $\tilde{\nu} = 3096$ (w, CH), 2968 (m, CH), 2932 (m, CH), 2871 (m, CH), 2555 (m, BH), 2004 (w, CO), 1884 cm^{-1} (vs, CO); ESI-MS: m/z: 728.4 [Tp$^#$Ni(Py−tBu)]; elemental analysis calcd (%) for $C_{46.5}H_{59}O_4N_9$-$BBr_3ClCoNi$ (6^{Ni}·CH$_2$Cl$_2$): C 46.10, H 4.91, N 10.40; found: C 46.60, H 5.27, N 10.37.

Data for $6'^{Co}$: Red-purple crystals; IR: $\tilde{\nu} = 2967$ (m, CH), 2871 (w, CH), 2554 (w, BH), 2003 (w, CO), 1884 (vs, CO), 1615 cm^{-1} (s, Py); ESI-MS: m/z: 727.4 [Tp$^#$Co(pyt^{Bu})]; elemental analysis calcd (%) for $C_{46.9}H_{59.8}O_4N_9BBr_3Cl_{1.8}Co_2$ ($6'^{Co}$·(CH$_2$Cl$_2$)$_{0.9}$): C 45.22, H 4.84, N 10.12; found: C 44.88, H 5.12, N 10.66.

Data for $7'^{Ni}$: Yellow crystals (crystallized from CH$_2$Cl$_2$/toluene/Et$_2$O); IR: $\tilde{\nu} = 3060$ (w, CH), 2953 (m, CH), 2929 (m, CH), 2862 (w, CH), 2545 (w, BH), 2004 (w, CO), 1884 cm^{-1} (vs, CO); ESI-MS: m/z: 799.3 [Tp$^#$Ni-(OCC$_2$Ph$_2$)]; elemental analysis calcd (%) for $C_{64}H_{49}O_7N_6BBr_3CoNi$: C 55.61, H 3.57, N 6.08; found: C 54.97, H 3.37, N 5.98.

Data for $7'^{Co}$: Yellow crystals (crystallized from CH$_2$Cl$_2$/toluene/Et$_2$O); IR: $\tilde{\nu} = 3060$ (m, CH), 2960 (m, CH), 2926 (m, CH), 2859 (w, CH), 2546 (m, BH), 1980 (w, CO), 1887 cm^{-1} (vs, CO); ESI-MS: m/z: 799.3 [Tp$^#$Co-(OCC$_2$Ph$_2$)]; elemental analysis calcd (%) for $C_{64.5}H_{50}O_7N_6BBr_3ClCo_2$ ($7'^{Co}$·(CH$_2$Cl$_2$)$_{0.5}$): C 54.37, H 3.54, N 5.90; found: C 54.83, H 3.73, N 5.73.

Data for $8'^{Ni}$: Pale green crystals (crystallized from CH$_2$Cl$_2$/hexane); IR: $\tilde{\nu} = 3107$ (m, CH), 2961 (w, CH), 2926 (w, CH), 2545 (m, BH), 2002 (w, CO), 1876 cm^{-1} (vs, CO); ESI-MS: m/z: 702.3 [Tp$^#$Ni(PyO^{Me})]; elemental analysis calcd (%) for $C_{37}H_{40}O_7N_9BBr_3CoNi$: C 40.74, H 3.70, N 11.56; found: C 40.92, H 3.75, N 11.28.

Data for $8'^{Co}$: Orange crystals (crystallized from CH$_2$Cl$_2$/hexane); IR: $\tilde{\nu} = 3112$ (w, CH), 3042 (w, CH), 2970 (w, CH), 2929 (w, CH), 2002 (w, CO), 1874 cm^{-1} (vs, CO); ESI-MS: m/z: 703.4 [Tp$^#$Co(Py^{Me}O)]; elemental analysis calcd (%) for $C_{41}H_{49}O_7N_9BBr_3Cl_2Co_2$ ($8'^{Co}$·(CH$_2$Cl$_2$)(hexane)$_{0.5}$): C 40.39, H 4.05, N 10.34; found: C 40.47, H 3.65, N 10.62.

Data for $9'^{Ni}$: Yellow green crystals (reaction in toluene; crystallized from toluene/hexane); IR: $\tilde{\nu} = 3006$ (w, CH), 2961 (w, CH), 2918 (w, CH), 2552 (m, BH), 2006 (w, CO), 1876 cm^{-1} (vs, CO); elemental analysis calcd (%) for $C_{25}H_{39}O_8N_6S_3BBr_3CoNi$ ($9'^{Ni}$·DMSO): C 29.56, H 3.87, N 8.27; S 9.47; found: C, 29.72; H, 3.93; N, 8.19; S, 9.58.

Data for $9'^{Co}$: Pink crystals (reaction in toluene; crystallized from toluene/hexane): IR: $\tilde{\nu} = 3006$ (w, CH), 2957 (w, CH), 2918 (w, CH), 2548 (w, BH), 2006 (m, CO), 1885 cm^{-1} (vs, CO).

Data for $10'a^{Ni}$: Orange crystals (reaction in toluene; crystallized from toluene/hexane). IR: $\tilde{\nu} = 3122$ (w, CH), 3079 (w, CH), 3024 (w, CH), 2959 (m, CH), 2928 (m, CH), 2870 (w, CH), 2548 (m, BH), 2006 (w, CO), 1879 cm^{-1} (vs, CO); ESI-MS: m/z: 749.3 [Tp$^#$Ni(bipy)]; elemental analysis calcd (%) for $C_{29}H_{27}O_4N_8BBr_3CoNi$: C 37.87, H 2.96, N, 12.18; found: C 37.42, H 4.06, N 11.17.

Data for $10b^{Ni}$: Orange crystals (reaction in toluene; crystallized from toluene): IR: $\tilde{\nu} = 2961$ (w, CH), 2924 (w, CH), 2546 (w, BH), 2006 (w, CO), 1887 (vs, CO), 1828 cm^{-1} (m, sh, CO); ESI-MS: m/z: 777.4 [Tp$^#$Ni-(bipy^{Me2})]; elemental analysis calcd (%) for $C_{31}H_{33}O_4N_8BBr_3CoNi$: C 39.20, H 3.50, N 11.80; found: C 38.98, H 3.74, N 11.38.

Reaction of 1 and $1'$ with soft donors—formation of $11'a$: First, dppe (53 mg, 0.131 mmol) was added to a solution of 1^{Ni} (100 mg, 0.131 mmol) in CH$_2$Cl$_2$ (10 mL), and then the resultant mixture was stirred for 2 h. Removal of the volatiles under reduced pressure followed by crystallization from CH$_2$Cl$_2$/Et$_2$O gave $11'a$ as brown crystals (71 mg, 0.062 mmol, 48% yield). ^1H NMR (500 MHz, [D_8]THF, 25°C, TMS): $\delta = 7.67$ (t, ^3J-(H,H) = 8.5 Hz, 8H; Ph), 7.46 (t, ^3J(H,H) = 7 Hz, Ph), 7.40 (t, ^3J(H,H) = 7 Hz, Ph), 2.55 (d, ^2J(H,P) = 14.5 Hz, 4H; PCH$_2$), 2.25 (s, 9H; Me), 1.89 ppm (br s, 9H; Me); ^{13}C NMR (125 MHz, [D_8]THF, 25°C, TMS): $\delta = 147.9$, 141.5 (2s, pz), 135–120 (Ph signals), 95.4 (4-pz), 31.9 (t, ^2J(C,P) = 22 Hz, PCH$_2$), 13.0, 11.6 ppm (2s, Me); ^{31}P NMR (202 MHz, [D_8]THF, 25°C, H$_3$PO$_4$): $\delta = 62.1$ ppm; IR: $\tilde{\nu} = 3053$ (w, CH), 2964 (w, CH), 2932 (m, CH), 2856 (m, CH), 2534 (w, BH), 1960 (m, CO), 1889 (m, CO), 1812 (s, CO), 1777 cm^{-1} (vs, CO); elemental analysis calcd (%) for $C_{46}H_{48}O_{3.5}N_6P_2BBr_3CoNi$ ($11'a$·(Et$_2$O)$_{0.5}$): C 47.18, H 4.13, N 7.18; found: C 47.40, H 4.14, N 6.79.

Reaction of 1^{Ni} and 1^{Co} with soft donors: Reaction of 1^{Ni} with dppene (dppene = *cis*-1,2-bis(diphenylphosphino)ethene)) and reaction of 1^{Co} with dppe were carried out in a manner similar to the preparation of $11'a$.

Data for $11'b$: Brown crystals; ^1H NMR (270 MHz, [D_8]THF, 25°C, TMS): $\delta = 7.70$ (t, ^3J(H,H) = 8.4 Hz, 8H; Ph), 7.47–7.40 (m, 12H; Ph), 7.30–7.19 (m, 2H; =CH), 2.28 (s, 9H; Me), 1.91 ppm (br s, 9H; Me);

^{13}C NMR (67.8 MHz, [D$_8$]THF, 25°C, TMS): $\delta = 149.6$ (d, ^2J(C,P) = 150 Hz, P-CH), 148.2, 141.9 (s×2, pz), 134.3 (d, ^3J(C,P) = 6 Hz, o-Ph), 134.0 (d, ^2J(C,P) = 2.4 Hz, ipso-Ph), 131.5 (p-Ph), 129.6 (t, ^4J(C,P) = 10 Hz, m-Ph), 95.7 (4-pz), 13.8, 11.9 ppm (2s, Me); ^{31}P NMR (202 MHz, [D$_8$]THF, 25°C, H$_3$PO$_4$): $\delta = 61.84$ ppm (br); IR: $\tilde{v} = 3075$ (w, CH), 3065 (w, CH), 2967 (m, CH), 2923 (w, CH), 2853 (w, CH), 2528 (m, BH), 1965 (vs, CO), 1812 (vs, CO), 1775 cm^{-1} (vs, CO); elemental analysis calcd (%) for C$_{46}$H$_{46}$O$_{3.5}$N$_6$P$_2$BBr$_3$CoNi (11'b·(Et$_2$O)$_{0.5}$): C 47.26, H 3.97, N 7.19; found: C 47.14, H 4.06, N 6.80.

Data for **12**: Identified on the basis of its IR feature (a hybrid of the structurally characterized [Co(CO)(dppe)$_2$]OTf[54] and PPN[Co(CO)$_4$] and the ESI-MS spectrum containing the peaks for the cationic part.

Formation of **13′**: *tert-*Butylisonitrile (28 μL, 0.131 mmol) was added to a solution of **1′^{Ni}** (100 mg, 0.131 mmol) in toluene (5 mL), and the resultant mixture was stirred for 1 h. Removal of the volatiles under reduced pressure followed by crystallization from toluene/hexane gave **13′** as deep red crystals (91 mg, 0.10 mmol, 77% yield). ^{1}H NMR (270 MHz, [D$_8$]THF, 25°C, TMS): $\delta = 2.41$, 2.33 (2s, 18H; Me), 1.56, 1.50 ppm (2s, 18H (2:1); Me); ^{13}C NMR (67.8 MHz, [D$_8$]THF, 25°C, TMS): $\delta = 147.0$, 140.9 (pz), 94.4 (4-pz), 57.3 (CMe$_3$), 30.0, 29.7 (CMe$_3$), 12.7, 10.6 (Me); (−90°C) 239.2 (μ-CO), 198.5 (br s, CO), 146.9 (3 or 5-pz), 145.6 (C≡N), 144.5 (3 or 5-pz′), 94.4, 94.0 (4-pz), 57.5, 29.2 (CMe$_3$), 14.1, 10.9, 10.8, 10.4 ppm (Me(pz)); IR: $\tilde{v} = 2980$ (m, CH), 2928 (w, CH), 2862 (w, CH), 2539 (w, BH), 2169 (vs, CN), 2142 (vs, CN), 2003 (vs, CO), 1831 (vs, CO), 1801 (vs, CO), 1775 ppm (s, CO); elemental analysis calcd (%) for C$_{28}$H$_{37}$O$_3$N$_8$BBr$_3$CoNi: C 37.29, H 4.14; N 12.43; found: C 37.41, H 4.38, N 12.22.

Formation of **14**: Because the reaction of **1′^{Co}** gave only a trace amount of crystals, compound **14** was characterized only by X-ray crystallography (SI 35[13]).

Formation of **15′**: Diphenylacetylene (47 mg, 0.262 mmol) was added to a solution of **2′^{Ni}** (100 mg, 0.131 mmol) in toluene (10 mL) and the resultant mixture was stirred for 2 d. Concentration followed at −30°C gave **15′** as brown crystals (10 mg, 0.011 mmol, 9% yield). IR: $\tilde{v} = 3053$ (w, CH), 2961 (w, CH), 2922 (w, CH), 2526 (w, BH), 2057 (vs, CO), 2005 cm^{-1} (vs, CO).[53]

Reaction of 3′ with hard donors: Upon addition of 3 equivalents of donor to a solution of **3′** (100 mg, 0.123 mmol) in CH$_2$Cl$_2$ (10 mL), the solution turned green. After concentration under reduced pressure hexane was added and the mixture was cooled at −30°C to give the green product.

Data for **17′a**: IR: $\tilde{v} = 3082$ (w, CH), 2961 (vs, CH), 2928 (vs, CH), 2869 (s, CH), 2526 (m, BH), 1614 ppm (vs, py); elemental analysis calcd (%) for C$_{33}$H$_{45}$N$_8$BBr$_3$ClNi: C 44.12, H 5.05, N 12.47, Br 26.68, Cl 3.95; found: C 44.48, H 5.05, N 12.47, Cl 3.95, Br 25.86.

Data for **17′b**: IR: $\tilde{v} = 3104$ (w, CH), 3071 (w, CH), 3052 (w, CH), 3028 (m, CH), 2957 (m, CH), 2927 (m, CH), 2545 (m, BH), 1606 (s, py), 1601 cm^{-1} (s, py); elemental analysis calcd (%) for C$_{25}$H$_{27}$N$_8$BBr$_3$ClNi: C 38.29, H 3.47, N 14.29, Br 30.57, Cl 4.52; found: C 37.94, H 3.53, N 13.84, Br 28.12, Cl 4.75.

Data for **17′c**: IR: $\tilde{v} = 3101$ (w, CH), 3073 (w, CH), 3039 (w, CH), 2959 (w, CH), 2924 (w, CH), 2514 (m, BH), 1637 (m, py), 1612 (m, py); elemental analysis calcd (%) for C$_{28.25}$H$_{35.5}$O$_2$N$_8$BBr$_3$Cl$_{3.5}$Ni (17′c·(CH$_2$Cl$_2$)$_{1.25}$): C 35.63, H 3.76, N 11.76; found: C 35.95, H 4.21, N 11.39.

Data for **17′d**: IR: $\tilde{v} = 3109$ (w, CH), 3070 (w, CH), 3041 (w, CH), 2955 (w, CH), 2925 (w, CH), 2855 (w, CH), 2511 (m, BH), 1861 (s, CO), 1602 (vs, C=C), 1585 (vs, C=C), 1572 cm^{-1} (s, C=C).[53]

Reaction of 3′ with soft donors—formation of 18′a: A solution of **3′** in CH$_2$Cl$_2$ (10 mL) was stirred for 2 h under a CO atmosphere (1 atm). Concentration under reduced pressure and addition of hexane followed by cooling −30°C gave **18′a** as deep brown crystals (35 mg, 12 mmol, 34% yield). ^{1}H NMR (270 MHz, [D$_2$]CH$_2$Cl$_2$, 25°C, TMS): $\delta = 5.61$ (s, 5H; Cp), 2.35 ppm (s, 18H; Me); ^{13}C NMR (67.8 MHz, [D$_2$]CH$_2$Cl$_2$, 25°C, TMS): $\delta = 147.8$, 142.7 (2s, pz), 96.0 (4-pz), 88.5 (Cp), 11.9 ppm (Me); IR: $\tilde{v} = 3119$ (w, CH), 3107 (w, CH), 2963 (m, CH), 2926 (m, CH), 2533 (m, BH), 2013 (vs, CO), 2003 (vs, CO), 1858 (s, CO), 1846 (s, CO), 1815 (vs, CO), 1801 cm^{-1} (vs, CO); elemental analysis calcd (%) for

C$_{23}$H$_{24}$O$_3$N$_6$BBr$_3$NiRu; C 32.78, H 2.87, N 9.97; found: C 32.73, H 3.02, N 10.06.

Formation for **18′b**: Compound **18′b** was prepared by a procedure similar to that decribed for **18′a**, and its analytically pure samples was obtained by the reaction with Cy−N=C=S (see below).

Data of **18′c**: ^{1}H NMR (270 MHz, [D$_2$]CH$_2$Cl$_2$, 25°C, TMS): $\delta = 5.39$ (s, 5H; Cp), 2.34 (br s, 15H; Me), 1.54 (s, 3H; Me), 1.47 ppm (s, 9H; tBu); ^{1}H NMR (270 MHz, [D$_2$]CH$_2$Cl$_2$, −90°C, TMS): $\delta = 5.37$ (s, 5H; Cp), 2.31, 2.24 (2s, 12H; Me), 1.85 (s, 3H; Me), 1.39 ppm (s, 12H; Me, tBu); ^{13}C NMR (67.8 MHz, [D$_2$]CH$_2$Cl$_2$, 25°C, TMS): $\delta = 244.9$ (CO), 147.5, 142.1 (2s, pz), 95.6 (4-pz), 86.3 (Cp), 32.0, 31.0 (s×2, CMe$_3$), 11.7 ppm (Me); IR: $\tilde{v} = 3104$ (w, CH), 2979 (m, CH), 2959 (m, CH), 2933 (m, CH), 2865 (w, CH), 2521 (m, BH), 2145 (s, CN), 1836 (m, CO), 1830 (m, CO), 1786 cm^{-1} (vs, CO); elemental analysis calcd (%) for C$_{28}$H$_{35}$O$_2$N$_7$BBr$_3$Cl$_2$NiRu (18′c·CH$_2$Cl$_2$): C 34.22, H 3.59, N 9.98; found: C 34.32; H 3.26; N 9.54.

Formation for **18′d**: A suspension containing **3′** (100 mg, 0.123 mmol) and PPh$_3$ (32 mg, 0.184 mmol) in toluene (10 mL) was sonicated for 1 h with an ultrasonic bath to get a homogeneous solution, which was further stirred for 2 h. Concentration under reduced pressure followed by crystallization after addition of hexane gave **18′d** as orange crystals (34 mg, 0.032 mmol, 24% yield). ^{1}H NMR (500 MHz, [D$_8$]THF, 25°C, TMS): $\delta = 7.69$ (t, ^3J(H,H) = 8 Hz, 6H; m-Ph), 7.43 (t, ^3J(H,H) = 7 Hz, 9H; o-, p-Ph), 4.92 (s, 5H; Cp), 2.22, 2.04 ppm (2s, 18H; Me); ^{13}C NMR (125 MHz, [D$_8$]THF, 25°C, TMS): $\delta = 242.8$ (d, ^2J(C,P) = 12.2 Hz, μ-CO), 148.4 (3 or 5-pz), 142.8 (3 or 5-pz), 136.8 (d, ^1J(C,P) = 46.5 Hz, ipso-Ph), 135.4 (d, ^2J-(C,P) = 11.3 Hz, Ph), 131.5 (p-Ph), 129.4 (d, ^2J(C,P) = 10.1 Hz, Ph), 96.4 (4-pz), 89.6 (Cp), 14.8, 14.3, 12.2 ppm (3s, Me); ^{31}P NMR (202 MHz, [D$_8$]THF, 25°C, H$_3$PO$_4$): $\delta = 46.5$ ppm; IR: $\tilde{v} = 3107$ (w, CH), 3052 (w, CH), 2956 (m, CH), 2925 (m, CH), 2865 (w, CH), 2472 (m, BH), 1962 (m, CO), 1821 (w, CO), 1772 cm^{-1} (vs, CO); satisfactory elemental analysis results could not be obtained due to the extreme sensitivity of **18′d**, which decomposed upon exposure to the air to give a product formulated as [Tp#Ni(κ^2-(O,O)O$_2$C)RuCp(CO)(PPh$_3$)]: IR: $\tilde{v} = 3053$ (w, CH), 2955 (m, CH), 2927 (m, CH), 2854 (w, CH), 2522 (m, BH), 1958 cm^{-1} (vs, CO); elemental analysis calcd (%) for C$_{40}$H$_{39}$O$_3$N$_6$PBBr$_3$NiRu: C 43.95, H 3.60, N 7.69; found: C 43.58, H 3.88, N 7.14.

Formation of **19′**: A solution of **3′** and phenylacetylene (100 μL, 0.91 mmol) in CH$_2$Cl$_2$ (10 mL) was stirred for 3 h. Concentration and crystallization from CH$_2$Cl$_2$/hexane gave **19′** as deep purple crystals (22 mg, 0.0245 mmol, 20% yield). ^{1}H NMR (270 MHz, [D$_8$]THF, 25°C, TMS): $\delta = 7.28$ (d, ^3J(H,H) = 7.0 Hz, 2H; o-Ph), 7.19 (t, ^3J(H,H) = 7.83 Hz, 2H; m-Ph), 7.02 (t, ^3J(H,H) = 7.0 Hz, 1H; p-Ph), 5.86 (s, 5H; Cp), 5.32 (s, 1H; =CH), 2.46, 2.41, 2.36, 2.28, 1.94, 1.73 ppm (6s, 18H; Me); ^{13}C NMR (67.8 MHz, [D$_8$]THF, 25°C, TMS): $\delta = 251.7$ (>C=), 148.9 (pz), 142.9 (pz), 137.0 (=CH), 135.0 (ipso-Ph), 129.5 (o-Ph), 126.6 (m-Ph), 126.4 (p-Ph), 96.5 (4-pz), 90.6 (Cp), 15.0, 12.4 ppm (2s, Me); IR: $\tilde{v} = 3053$ (w, CH), 3017 (w, CH), 2968 (m, CH), 2926 (m, CH), 2854 (m, CH), 2524 (m, BH), 2017 (vs, CO), 1843 (vs, CO), 1588 (s, C=C), 1568 (m, C=C); elemental analysis calcd (%) for C$_{37}$H$_{46}$O$_2$N$_6$BBr$_3$Cl$_2$NiRu (19′·CH$_2$Cl$_2$·hexane): C 40.85, H 7.72; found: C 40.80, H 4.31, N 7.86.

Reaction of 3′ with isothiocyanate—reaction with Cy−N=C=S: Cyclohexylisocyanide (30 mL, 0.123 mmol) was added to a solution of **3′** (100 mg, 0.123 mmol) in CH$_2$Cl$_2$ (10 mL) and the resultant mixture was stirred for 3 h. Concentration and crystallization from CH$_2$Cl$_2$/hexane gave **18′b** as deep red crystals (13 mg, 0.014 mmol, 23% yield). Concentration of the supernatant solution and cooling gave **20′b** as green crystals (24% yield).

Data for **18′b**: ^{1}H NMR (270 MHz, [D$_2$]CH$_2$Cl$_2$, 25°C, TMS): $\delta = 5.40$ (s, 5H; Cp), 3.84 (br, 1H; Cy), 2.33 (s, 18H; Me), 1.91–1.40 ppm (m, 10H; Cy); ^{13}C NMR (67.8 MHz, [D$_2$]CH$_2$Cl$_2$, 25°C, TMS): $\delta = 147.6$ (s, 3 or 5-pz), 142.1 (s, 3 or 5-pz), 95.7 (s, 4-pz), 86.3 (s, Cp), 33.3, 25.3, 23.4 (s×3, CH$_2$), 11.8 ppm (s, Me); IR: $\tilde{v} = 2934$ (m, CH), 2852 (w, CH), 2519 (w, CH), 2173 (s, CN), 1986 (w, CO), 1842 (s, CO), 1793 cm^{-1} (vs, CO); elemental analysis calcd (%) for C$_{29.5}$H$_{36}$O$_2$N$_7$BBr$_3$ClNiRu (18′b·(CH$_2$Cl$_2$)$_{0.5}$): C 36.66, H 3.75, N 10.15; found: C, 36.90; H, 3.81; N, 10.15.

Data for **20′b**: IR: $\tilde{v} = 2959$ (w, CH), 2923 (m, CH), 2851 (m, CH), 2532 (m, BH), 2039 (vs, CO), 1986 cm^{-1} (vs, CO); elemental analysis calcd

(%) for $C_{29.5}H_{36}O_2N_7S_2BBr_3ClNiRu$ (**20′b·(CH_2Cl_2)_{0.5}**): C 34.38, H 3.52, N 9.51, S 6.22; found: C 34.59, H 3.55, N 9.65, S 5.83.

Reaction of 3′ with isothiocyanate—reaction with Ph−N=C=S: The reaction was carried out in a manner similar to the reaction with Cy−NCS.

Data for 18′e: ^1H NMR (270 MHz, [D_2]CH_2Cl_2, 25 °C, TMS): $\delta = 7.31$ (br, 5H; Ph), 5.55 (s, 5H; Cp), 2.35 ppm (s, 18H; Me); ^{13}C NMR (67.8 MHz, [D_2]CH_2Cl_2, 25 °C, TMS): $\delta = 147.8$ (pz), 142.3 (pz), 129.7 (br s, Ph), 95.8 (4-pz), 87.3 (s, Cp), 14.1, 11.8 ppm (2 s, Me); IR: $\tilde{v} = 3065$ (w, CH), 2959 (m, CH), 2926 (m, CH), 2536 (m, BH), 2137 (vs, CN), 1994 (m, CO), 1832 (vs, CO), 1788 cm^{-1} (vs, CO); elemental analysis calcd (%) for $C_{29}H_{29}O_2N_7BBr_3NiRu$: C 37.95, H 3.18, N 10.68; found: C 37.75, H 3.51, N 10.47.

Data for 20′e: $\tilde{v} = 3085$ (w, CH), 2951 (m, CH), 2924 (m, CH), 2855 (w, CH), 2521 (m, BH), 2045 (vs, CO), 1996 (vs, CO), 1986 cm^{-1} (vs, CO); elemental analysis calcd (%) for $C_{30.5}H_{32.5}O_2N_7S_2BBr_3NiRu$ (**20′e·(hexane)_{0.25}**): C 36.50, H 3.26, N 9.77, S 6.39; found; C 36.51, H 3.54, N 9.40, S 6.33.

X-ray crystallography: Thirty-three complexes were characterized by X-ray crystallography. Diffraction measurements were made on a Rigaku RAXIS IV imaging plate area detector with Mo$_{K\alpha}$ radiation ($\lambda = 0.71069$ Å). All data collections were carried out at -60 °C. Neutral scattering factors were obtained from the standard source.[55a] In the reduction of data, Lorentz, polarization, and empirical absorption corrections were made.[55b] The structures were solved by a combination of the direct methods (SHELXL 86)[55c] and Fourier synthesis (DIRDIF).[55e] Least-squares refinements were carried out using SHELEXL 97[55d] linked to teXsan.[55f] For crystallographic data and details of structure refinements, see the Supporting Information (SI 10 and 11[13]). CCDC-252176 (**B**), CCDC-252177 (**C**), CCDC-164175 (**1^Ni**), CCDC-164176 (**1^Co**), CCDC-252178 (**1^Fe**), CCDC-175901 (**1^Mn**), CCDC-175902 (**1′^Ni**), CCDC-252179 (**1′^Co**), CCDC-164178 (**2^Ni**), CCDC-211846 (**3′**), CCDC-252180 (**2^Co**), CCDC-252181 (**2^Fe**), CCDC-252182 (**2^Mn**), CCDC-252183 (**2′^Ni**), CCDC-252184 (**5′**), CCDC-252185 (**6′^Ni**), CCDC-252186 (**7′^Ni**), CCDC-252187 (**8′^Ni**), CCDC-252188 (**9′^Ni**), CCDC-252189 (**10′b^Ni**), CCDC-252190 (**11′a**), CCDC-252191 (**13′**), CCDC-252192 (**14**), CCDC-252193 (**15′**), CCDC-252194 (**16′**), CCDC-252195 (**17′b_2·D_{1/2}**), CCDC-252196 (**17′c**), CCDC-252197 (**18′a**), CCDC-252198 (**18′b**), CCDC-211848 (**18′d**), CCDC-211849 (**19′**), CCDC-252199 (**20′b**), and CCDC-252200 (**20′c**) contain the supplementary crystallographic data for this paper. These data can be obtained free of charge from The Cambridge Crystallographic Data Centre via www.ccdc.cam.ac.uk/data_request/cif.

DFT calculations: Model complexes [Tp^{H_2}Ni−Co(CO)_4] (**E**; triplet; C_3 symmetry), [Tp^{H_2}Ni−Co(CO)_4] (**E′**; singlet), [Tp^{H_2}Ni−Co(CO)_3(PH_3)] (**F**; triplet; C_1 symmetry), [Tp^{H_2}Ni−RuCp] (**G**; triplet; C_1 symmetry) (Tp^{H_2} = hydrotris(pyrazolyl)borato) for the corresponding xenophilic complexes were subjected to DFT calculations. Initial structures for the model complexes were based on the coordinates obtained from the X-ray crystallographic data of [Tp^{iPr_2}Ni−Co(CO)_4] (**1′^Ni**), [Tp$^#$Ni−Co(CO)_3(PPh_3)] (**2′^Ni**), and [Tp$^#$Ni−RuCp(CO)_2] (**3′^Ni**). The structures were determined by gradient optimization using the Gaussian 98 package (Revision A.11)[56a] at the B3LYP density functional level.[56b,c] All metal centers (Ni, Co, and Ru), three Tp nitrogen atoms coordinated to the metal, and the phosphorus atom in **F** were described with a lanl2dz basis set of valence double-ζ quality including relativistic effective core potential of Hay and Wadt.[56d–f] The 3–21 G split-valence basis set was used for the other atoms. DFT calculations were also performed for the reference complexes, [Li−Co(CO)_4] (**H**) and [CH_3−Co(CO)_4] (**I**). C_3 symmetry was assumed for **I**.

Acknowledgements

[1] *Comprehensive Organometallic Chemistry II*, *Vol. 10* (Eds.: E. W. Abel, F. G. A., Stone, G. Wilkinson), Pergamon: Oxford, **1995**; *The Chemistry of Metal Cluster Complexes* (Eds.: D. F. Shriver, H. D. Kaesz, R. D. Adams), VCH, New York, **1990**; *Metal Clusters in Chemsitry* (Eds.: P. Braunstein, L. A. Oro, P. R. Raithby), Wiley-VCH, Weinheim, **1999**; P. J. Dyson, J. S. McIndoe, *Transition Metal Carbonyl Cluster Chemistry*, Gordon and Breach Science, Amsterdam, **2000**.

[2] a) L. H. Gade, *Angew. Chem.* **2000**, *112*, 2768; *Angew. Chem. Int. Ed.* **2000**, *39*, 2659; b) N. Wheatley, P. Kalck, *Chem. Rev.* **1999**, *99*, 3379.

[3] a) B. R. Whittlesey, *Coord. Chem. Rev.* **2000**, *206/207*, 395; b) G. Fachinetti, G. Fochi, T. Funaioli, P. F. Zanazzi, *J. Chem. Soc. Chem. Commun.* **1987**, 89; c) G. Fachinetti, G. Fochi, T. Funaioli, P. F. Zanazzi, *Angew. Chem.* **1987**, *99*, 681; *Angew. Chem. Int. Ed. Engl.* **1987**, *26*, 680; d) C. Meali, M. Proserpio, G. Fachinetti, T. Funaioli, G. Fochi, P. F. Zanazzi, *Inorg. Chem.* **1989**, *28*, 1122; e) T. Funaioli, P. Biagini, P. F. Zanazzi, G. Fachinetti, *Gazz. Chim. Ital.* **1991**, *121*, 321; f) G. Kong, G. N. Harakas, B. R. Whittlesey, *J. Am. Chem. Soc.* **1995**, *117*, 3502; g) G. N. Harakas, B. R. Whittlesey, *J. Am. Chem. Soc.* **1996**, *118*, 4210; h) L. H. Gade, *Angew. Chem.* **1996**, *108*, 2225; *Angew. Chem. Int. Ed. Engl.* **1996**, *35*, 2089; i) Z. Xu, Z. Lin, *Chem. Eur. J.* **1998**, *4*, 28; See also reference [2a] and W. Hieber, *Adv. Organomet. Chem.* **1970**, *8*, 1.

[4] In this paper discussion will be focused on paramagnetic complexes, although "xenophilic" complexes are not always so according to the definition. The metal–metal interaction in diamagnetic xenophilic complexes may be described as a polarized covalent single bond like those in ELHB complexes (Scheme 8).

[5] R. H. Crabtree, *The Organometallic Chemistry of the Transition Metals*, 3rd ed., Wiley-Interscience, New York, **2001**; B. Cornils, W. Herrmann, *Applied Homogeneous Catalysis with Organometallic Compounds (2 Vols.)*, VCH, Oxford, **1996**.

[6] M. Akita, S. Hikichi, *Bull. Chem. Soc. Jpn.* **2002**, *75*, 1657.

[7] S. Trofimenko, *Scorpionates The Coordination Chemistry of Polypyrazolylborate Ligands*, Imperial College Press, London, **1999**; S. Trofimenko, *Chem. Rev.* **1993**, *93*, 943; N. Kitajima, W. B. Tolman, *Prog. Inorg. Chem.* **1995**, *43*, 419.

[8] M. Akita, N. Shirasawa, S. Hikichi, Y. Moro-oka, *Chem. Commun.* **1998**, 973; N. Shirasawa, M. Akita, S. Hikichi, Y. Moro-oka, *Chem. Commun.* **1999**, 417; N. Shirasawa, M. Akita, S. Hikichi, Y. Moro-oka, *Organometallics* **2001**, *20*, 3582; S. Yoshimitsu, S. Hikichi, M. Akita, *Organometallics* **2002**, *21*, 3762.

[9] Dinuclear complexes with bridging ligands or coordinatively saturated [Tp^{R}ML$_n$] type fragments: see, for example, a) M. D. Curtis, K.-B. Shiu, W. M. Butler, J. C. Huffman, *J. Am. Chem. Soc.* **1986**, *108*, 3335; b) Y.-Y. Liu, A. Mar, S. J. Rettig, A. Storr, J. Trotter, *Can. J. Chem.* **1988**, *66*, 1997; c) K. B. Shiu, W.-N. Guo, S.-M. Peng, M.-C. Cheng, *Inorg. Chem.* **1994**, *33*, 3010; d) M. C. Nicasio, M. Paneque, P. J. Perez, A. Pizzano, M. L. Poveda, L. Rey, S. Sirol, S. Taboada, M. Trujillo, A. Monge, C. Ruiz, E. Carmona, *Inorg. Chem.* **2000**, *39*, 180; a few [Tp^{R}M–M′L$_n$]-type dimetallic complexes, in which M and M′ are a main group metal and a transition metal, respectively, are known: e) D. L. Reger, S. S. Mason, A. L. Rheingold, B. S. Haggarty, F. P. Arnold, *Organometallics* **1994**, *13*, 5049; f) D. L. Reger, D. G. Garza, A. L. Rheingold, G. P. A. Yap, *Organometallics* **1998**, *17*, 3624; g) O. M. Abu Salah, M. I. Bruce, *Aust. J. Chem.* **1977**, *30*, 2291; [CpMo(H)_2CuTp] reported in this last reference might contain only the dative Mo→Cu bond, but the interaction mode of the hydride ligands (η^1 or μ) has been left unclarified.

[10] Abbreviations used in this paper: Tp^R: hydrotris(pyrazolyl)borato ligands; Tp^{iPr_2}: 3,5-diisopropylpyrazolyl derivative; Tp$^#$, Tp$^{Me_2,4-Br}$: 3,5-dimethyl-4-bromopyrazolyl derivative; Tp^{Ph,Me}: 3-phenyl-5-methyl derivative; Tp^{H_2}: the nonsubstituted parent ligand; pz^R: pyrazolyl group in Tp^R. Compound numbers without the name of the central

metal atom refer to a series of metal complexes of a certain structure and each metal derivative is specified by the superscript. The Tp# derivatives are indicated with ′ and compound numbers without ′ are for Tp^{iPr_2} derivatives. For example, 1$'^{Ni}$ and 2 stand for [Tp#Ni–Co(CO)$_4$] and the series of [Tp^{iPr_2}M–Co(CO)$_3$(PPh$_3$)], respectively.

[11] Preliminary results were reported as communications. K. Uehara, S. Hikichi, M. Akita, *Organometallics* 2001, 20, 5002; K. Uehara, S. Hikichi, M. Akita, *Chem. Lett.* 2002, 1198.

[12] Two of the products isolated from the Tp^{Ph,Me} system could be characterized by X-ray crystallography to be ionic species containing the [Co(CO)$_4$]$^-$ fragment as a counterion: the carbonatonickel cluster compound, [μ$_4$-Na[{Na(THF)}(μ-CO$_3$)(NiTp^{Ph,Me})]$_4$]$^+$[Co(CO)$_4$]$^-$ (B; SI 13$^{[13]}$) and the aquocobalt complex, [Tp^{Ph,Me}Co-(THF)(OH$_2$···THF)$_2$][Co(CO)$_4$] (C; SI 14$^{[13]}$). These products should be formed through the interaction of Tp^{Ph,Me}M–Cl with adventitious impurities (i.e., CO$_2$,NaOH and water) during the prolonged reaction time or work up instead of via the desired metal–metal bond formation.
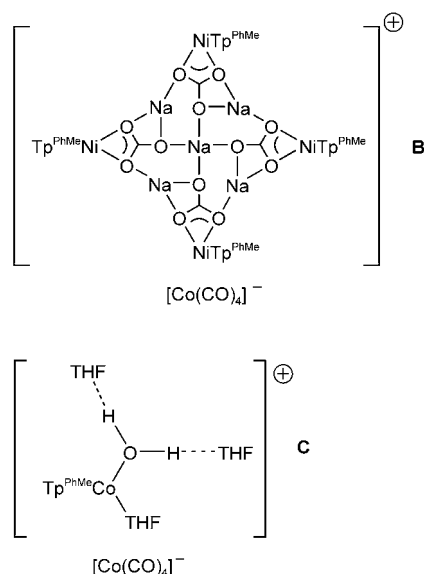
[13] The reference number in the Supporting Information.

[14] K. Uehara, S. Hikichi, M. Akita, *J. Chem. Soc. Dalton Trans.* 2002, 3529.

[15] We also examined synthesis of the Tp^{Ph,Me} derivatives from [Tp^{Ph,Me}M(NCMe)$_3$]PF$_6$,$^{[14]}$ but no characterizable product was obtained.

[16] a) G. G. Sumner, H. P. Klug, E. E. Alexander, *Acta Crystallogr.* 1964, 17, 732; P. C. Leung, P. Coppens, *Acta Crystallogr. Sect. B* 1983, 39, 535; b) K. H. Theopold, R. G. Bergman, *J. Am. Chem. Soc.* 1983, 105, 464; c) L. Brammer, J. C. M. Rivas, C. D. Spilling, *J. Organomet. Chem.* 2000, 609, 36.

[17] The molecular structure of [Co$_2$(CO)$_8$] determined by X-ray crystallography contains μ-CO ligands, [(OC)$_3$Co(μ-CO)$_2$Co(CO)$_3$] (Co–Co).$^{[16a]}$

[18] J. Emsley, *Elements*, 2nd ed., Oxford University Press, Oxford, 1998.

[19] K. Nakamoto, *Infrared and Raman Spectra of Inorganic and Coordination Compounds*, 5th ed., Wiley, New York, 1997.

[20] M. Akita, K. Ohta, Y. Takahashi, S. Hikichi, Y. Moro-oka, *Organometallics* 1997, 16, 4121.

[21] J. K, Ruff, W. J. Schlientz, *Inorg. Synth.* 1974, 15, 84.

[22] K. Inkrott, R. Goetze, S. G. Shore, *J. Organomet. Chem.* 1978, 154, 337.

[23] D. F. Shriver, P. W. Atkins, *Inorganic Chemistry*, 3rd ed., Oxford University Press, Oxford, 1999.

[24] See, for example, G. L. Geoffrey, M. S. Wrighton, *Organometallic Photochemistry*, Academic Press, New York, 1979; A. F. Heyduk, A. M. Macintosh, D. G. Nocera, *J. Am. Chem. Soc.* 1999, 121, 5023; and references therein.

[25] Reproducible results could not be obtained for the Fe and Mn complexes 1/1$'^{Fe,Mn}$ and 2/2$'^{Fe,Mn}$ due to their extreme sensitivity toward the air.

[26] a) L. H. Gade, H. Memmler, U. Kauper A. Schneider, S. Fabre, I. Bezougli, M. Lutz, C. Galka, U. J. Scowen, M. McPartlin, *Chem. Eur. J.* 2000, 6, 692; b) M. Lutz, M. Haukka, T. A. Pakkanen, L. H. Gade, *Organometallics* 2001, 20, 2631.

[27] D. G. Dick, D. W. Stephan, *Organometallics* 1990, 9, 1910; A. C. Street, Y. Mizobe, F. Gotoh, I. Mega, H. Oshita, M. Hidai, *Chem. Lett.* 1991, 383; G. E. Greco, M. B. O'Donoghue, S. W. Seidel, W. M. Davis, R. R. Schrock, *Organometallics* 2000, 19, 1132; see also references [3e,f]

[28] See for example, F. S. Stevens, *J. Chem. Soc. Dalton Trans.* 1974, 1067; B. H. Freeland, J. W. Hux, N. C. Payne, K. G. Tyers, *Inorg. Chem.* 1980, 19, 693.

[29] Y. Takahashi, M. Hashimoto, S. Hikichi, Y. Moro-oka, M. Akita, *Inorg. Chim. Acta* 2004, 357, 1711, and references therein.

[30] E. J. Moore, J. M. Sullivan, J. R. Norton, *J. Am. Chem. Soc.* 1986, 108, 2257; R. B. King, *Acc. Chem. Res.* 1970, 3, 417.

[31] We also examined reactions in THF but the reactions were so slow that concomitant decomposition of 3′ gave intractable mixtures of products.

[32] Compound D in the co-crystal contains only η^1-CO ligands [(η^1-CO)$_2$CpRu-RuCp(η^1-CO)$_2$; SI 38$^{[13]}$]. and the structure is in contrast to the previously reported structure with μ-CO, [Cp(CO)Ru(μ-CO)$_2$-RuCp(CO)] (Ru–Ru); T. Straub, M. Haukka, T. A. Pakkanen, *J. Organomet. Chem.* 2000, 612, 106. The former type of structure was reported for the derivatives with *ansa*-bis(cyclopentadienyl) ligands, for example, η^5-C$_5$R$_4$–(CH$_2$)$_n$-η^5–C$_5$R$_4$, but for the Cp derivative (D) only the latter structure was reported, although, in solution, the former structure can be detected by solution IR spectra. S. A. R. Knox, K. A. Macpherson, A. G. Orpen, M. C. Rendle, *J. Chem. Soc. Dalton Trans.* 1989, 1807; R. Boese, J. K. Cammack, A. J. Matzger, K. Pflug, W. B. Tolman, K. P. C. Vollhardt, T. W. Weidman, *J. Am. Chem. Soc.* 1997, 119, 6757; M. V. Ovchinnikov, D. P. Klein, I. A. Guzei, M.-G. Choi, R. J. Angelici, *Organometallics* 2002, 21, 617.

[33] Reaction of 3′ with dppm gave a mixture of [Ru$_2$Cp$_2$(μ-CO)$_2$(dppm)] and [Ni(Tp#)$_2$], which should arise from a redox process. The two products formed a co-crystal. Cell parameters for [Ru$_2$Cp$_2$(μ-CO)$_2$-(dppm)·Ni(Tp#)$_2$·CH$_2$Cl$_2$]: a = 35.2498(5), b = 10.9905(3), c = 31.5546(8), β = 113.541(1)°, V = 11207.2(5) Å^3.

[34] B. Mann, B. F. Taylor, ^{13}C NMR Data for Organometallic Compounds, Academic, New York, 1981.

[35] M. I. Bruce, *Chem. Rev.* 1998, 98, 2797.

[36] H. Werner, K. Leonhard, *Angew. Chem.* 1979, 91, 663; *Angew. Chem. Int. Ed. Engl.* 1979, 18, 627; M. D. Curtis, S. H. Druker, *J. Am. Chem. Soc.* 1997, 119, 1027; A. R. Manning, L. O'Dwyer, P. A. McArdle, D. Cunningham, *J. Organomet. Chem.* 1999, 573, 109.

[37] See the introductory part of the following paper. M. Akita, D.-q. Ma, S. Hikichi Y. Moro-oka, *J. Chem. Soc. Dalton Trans.* 1999, 987.

[38] U. Siemeling, U. Vorfeld, B. Neumann, H.-G. Stammler, *Organometallics* 1998, 17, 483; see also O. Schmitt, G. Wolmershäuser, H. Sitzmann, *Eur. J. Inorg. Chem.* 2003, 3105, and references therein.

[39] a) I. Nagy-Gergely, G. Szolntai, F. Ungvary, L. Marko, M. Moret, A. Sironi, C. Zucchi, A. Sisak, C. M. Tschoerner, Martinelli, A. Sorkau, G. Pályi, *Organometallics* 1997, 16, 2740; b) D Selent, R. Beckhaus, J. Pickardt, *Organometallics* 1993, 12, 2857; D. Selent, R. Beckhaus, T. Bartik, *J. Organomet. Chem.* 1991, 405, C15; c) C. Zucchi, A. Corma, R. Boese, E. Kelinpeter, H. Alper, G. Pályi, *J. Organomet. Chem.* 1999, 586, 61; d) S. Vastag, L. Markó, A. L. Rheingold, *J. Organomet. Chem.* 1989, 372, 141; e) M. A. Gafoor, A. T. Hutton, J. R. Moss, *J. Organomet. Chem.* 1996, 510, 233; f) I. P. Beletskaya, A. Z. Voskoboynikov, E. B. Chuklanova, N. I. Kirillova, A. K. Shestakova, I. N. Parshina, A. I. Gusev, G. K. I. Magomedov, *J. Am. Chem. Soc.* 1993, 115, 3156.

[40] A. Fukuoka, S. Fukagawa, M. Hirano, N. Koga, S. Komiya, *Organometallics* **2001**, *20*, 2065, and references therein.

[41] E. Hey-Hawkins, H. G. von Schnering, *Z. Naturforsch. B* **1991**, *45*, 621.

[42] a) Ab initio calculations for polynuclear Fe–Mn xenophilic complexes were reported: see references [3d,i]; b) A detailed MO calculation was performed for an ELHB complex: G. Jansen, M. Schubart, B. Findeis, L. H. Gade, I. J. Scowen, M. McPartlin, *J. Am. Chem. Soc.* **1998**, *120*, 7239.

[43] Colored figures of the molecular orbitals appearing in Figure 4 and Table 9 and in the charts are included in the Supporting Information.

[44] R. R. Schrock, K.-Y. Shih, D. A. Dobbs, W. M. Davis, *J. Am. Chem. Soc.* **1995**, *117*, 6609; J. L. Detrich, O. M. Reinaud, A. L. Rheingold, and K. H. Theopold, *J. Am. Chem. Soc.* **1995**, *117*, 11745.

[45] P. Z. Klufers, *Z. Kristallogr.* **1984**, 167, 253; P. Z. Klufers, *Z. Kristallogr.* **1984**, 167, 275.

[46] a) F. Calderazzo, G. Fachinetti, F. Marchetti, P. F. Zanazzi, *J. Chem. Soc. Chem. Commun.* **1981**, 181; b) Reference [16c] and references therein.

[47] a) D. A. Roberts, W. C. Mercer, G. L. Geoffroy, C. G. Pierpont, *Inorg. Chem.* **1986**, *25*, 1439; b) See also, P. Braunstein, J. Dehan, *J. Organomet. Chem.* **1970**, *24*, 497; c) Reference [39c].

[48] R. Poli, J. N. Harvey, *Chem. Soc. Rev.*, **2003**, *32*, 1; J.-L. Carreón-Macedo, J. N. Harvey, *J. Am. Chem. Soc.* **2004**, *126*, 5789.

[49] See for example, L. J. Farrugia, L. Mustoo, *Organometallics* **1992**, *11*, 2941, and references therein.

[50] R. G. Pearson, *J. Chem. Educ.* **1968**, *45*, 581; R. G. Pearson, *J. Chem. Educ.* **1968**, *45*, 643; R. G. Pearson, *Coord. Chem. Rev.* **1990**, *100*, 403; R. G. Pearson, *Chemical Hardness*, Wiley-VCH, New York, **1997**.

[51] a) N. Kitajima, K. Fujisawa, C. Fujimoto, Y. Moro-oka, S. Hashimoto, T. Kitagawa, K. Toriumi, K. Tatsumi, A. Nakamura, *J. Am. Chem. Soc.* **1992**, *114*, 1277; b) K. Uehara, S. Hikichi, M. Akita, *J. Chem. Soc. Dalton Trans.* **2002**, 3529; c) A. Albinati, M. Bovens, H. Rüegger, L. M. Venanzi, *Inorg. Chem.* **1997**, *36*, 5991.

[52] M. Brookhart, W. B. Studabaker, G. R. Husk, *Organometallics* **1987**, *6*, 1141.

[53] Analytically pure samples could not be obtained despite several attempts. Structures were characterized spectroscopically and/or crystallographically.

[54] K. Uehara, S. Hikichi, M. Akita, unpublished results.

[55] a) *International Tables for X-ray Crystallography, Vol. 4*, Kynoch Press, Birmingham, **1975**; b) T. Higashi, Program for Absorption Correction, Rigaku Corp., Tokyo, Japan, **1995**; c) G. M. Sheldrick, SHELXS-86: Program for crystal structure determination, University of Göttingen, Göttingen (Germany), **1986**; d) G. M. Sheldrick, SHELXL-97: Program for crystal structure refinement, University of Göttingen, Göttingen (Germany), **1997**; e) P. T. Beurskens, G. Admiraal, G. Beurskens, W. P. Bosman, S. Garcia-Granda, R. Gould, O. J. M. M. Smits, C. Smykalla, The DIRDIF program system, Technical Report of the Crystallography Laboratory, University of Nijmegen, Nijmegen (The Netherlands), **1992**; f) teXsan; Crystal Structure Analysis Package, version 1. 11, Rigaku Corp., Tokyo, Japan, **2000**.

[56] a) M. J. Frisch, G. W. Trucks, H. B. Schlegel, G. E. Scuseria, M. A. Robb, J. R. Cheeseman, V. G. Zakrzewski, J. A. Montgomery, Jr., R. E. Stratmann, J. C. Burant, S. Dapprich, J. M. Millam, A. D. Daniels, K. N. Kudin, M. C. Strain, O. Farkas, J. Tomasi, V. Barone, M. Cossi, R. Cammi, B. Mennucci, C. Pomelli, C. Adamo, S. Clifford, J. Ochterski, G. A. Petersson, P. Y. Ayala, Q. Cui, K. Morokuma, P. Salvador, J. J. Dannenberg, D. K. Malick, A. D. Rabuck, K. Raghavachari, J. B. Foresman, J. Cioslowski, J. V. Ortiz, A. G. Baboul, B. B. Stefanov, G. Liu, A. Liashenko, P. Piskorz, I. Komaromi, R. Gomperts, R. L. Martin, D. J. Fox, T. Keith, M. A. Al-Laham, C. Y. Peng, A. Nanayakkara, M. Challacombe, P. M. W. Gill, B. Johnson, W. Chen, M. W. Wong, J. L. Andres, C. Gonzalez, M. Head-Gordon, E. S. Replogle, J. A. Pople, *J. Chem. Phys.* **1993**, *98*, 5612; c) A. D. Becke, *J. Chem. Phys.* **1993**, *98*, 1372; d) P. J. Hay, W. R. Wadt, *J. Chem. Phys.* **1985**, *82*, 270; e) P. J. Hay, W. R. Wadt, *J. Chem. Phys.* **1985**, *82*, 299; f) W. R. Wadt, P. J. Hay, *J. Chem. Phys.* **1985**, *82*, 284.